NASA TECHNICAL NOTE

NASA TN D-2532

NASA TN D-2532

FLIGHT MEASUREMENTS OF STABILITY AND CONTROL DERIVATIVES OF THE X-15 RESEARCH AIRPLANE TO A MACH NUMBER OF 6.02 AND AN ANGLE OF ATTACK OF 25°

by Roxanah B. Yancey

Flight Research Center
Edwards, Calif.

OTS PRICE

XEROX $ 1.25 HC

MICROFILM $ 0.50 mf.

FLIGHT MEASUREMENTS OF STABILITY AND CONTROL DERIVATIVES

OF THE X-15 RESEARCH AIRPLANE TO A MACH NUMBER OF 6.02

AND AN ANGLE OF ATTACK OF 25°

By Roxanah B. Yancey

Flight Research Center
Edwards, Calif.

NATIONAL AERONAUTICS AND SPACE ADMINISTRATION

FLIGHT MEASUREMENTS OF STABILITY AND CONTROL DERIVATIVES OF THE

X-15 RESEARCH AIRPLANE TO A MACH NUMBER OF 6.02

AND AN ANGLE OF ATTACK OF 25°*

By Roxanah B. Yancey
Flight Research Center

SUMMARY

Flight tests of the X-15 airplane provided data from which longitudinal, lateral, and directional stability and control derivatives were determined over a Mach number range from 0.60 to 6.02 and over an angle-of-attack range from -2.7° to 25°. The data were obtained with the lower rudder on and off, speed brakes open and closed, and power on and off.

The longitudinal derivatives show the expected trends of increasing levels through the transonic region and diminishing levels as the Mach number increases in the supersonic region. A high level of longitudinal stability is indicated by the flight data.

When the lower rudder is on, the effective dihedral C_{l_β} has a positive trend with increasing Mach number and changes from a negative (favorable) value to a positive value at a Mach number of about 2.2. When the lower rudder is off, the favorable level of the effective dihedral and that of the directional cross-control derivative $C_{l_{\delta_V}}$ improve considerably. However, with the lower rudder removed, the level of the directional-stability derivative C_{n_β} and the level of the directional control derivative $C_{n_{\delta_V}}$ decrease substantially.

When the speed brakes are open, a favorable increment is added to the values of both the directional-stability derivative C_{n_β} and the side-force coefficient C_{Y_β}. Little effect of speed-brake deployment is noted on the effective dihedral C_{l_β}. No specific power effects are apparent on the trend of either the longitudinal or the lateral-directional data.

The derivatives obtained from flight data compare fairly well with wind-tunnel predictions for corresponding configurational and flight conditions. However, the flight data show a slightly higher longitudinal stability between a Mach number of 1.3 and 2.0 at the lower angles of attack and also reveal a

generally lower level in the directional parameters C_{n_β} and $C_{n_{\delta_v}}$ over the Mach number range investigated than predicted by the wind-tunnel data.

INTRODUCTION

During the expansion of the X-15 flight envelope, maneuvers have been performed to provide data from which to determine stability and control derivatives. The information obtained is used to update the X-15 simulator, which is instrumental in flight planning and pilot indoctrination, and to verify the aerodynamic characteristics predicted in wind-tunnel studies.

The initial flight-determined derivative study (ref. 1) was made with the interim Reaction Motors LR11 rocket engines over a Mach number range from 0.6 to 3.4 and for an angle-of-attack range from 0° to 15°. With the more powerful YLR99 engine, the study has been extended to a Mach number of 6.02 and an angle of attack of 25°. Data were obtained with the lower rudder on and off, speed brakes open and closed, and power on and off. This paper presents the results of both of the derivative studies and compares flight data with wind-tunnel predictions. The studies were made as part of a hypersonic flight program being conducted with the X-15 airplane by the National Aeronautics and Space Administration, the U.S. Air Force, and the U.S. Navy at the NASA Flight Research Center, Edwards, Calif.

SYMBOLS

The body system of axes is used.

a_n	normal acceleration at center of gravity, g units
a_t	transverse acceleration at center of gravity, g units
b	wing span, ft
C_l	rolling-moment coefficient, $\dfrac{\text{Rolling moment}}{\bar{q}Sb}$
C_{l_β}	lateral-stability derivative, $\dfrac{\partial C_l}{\partial \beta}$, per deg
$C_{l_{\delta_a}}$	aileron-effectiveness derivative, $\dfrac{\partial C_l}{\partial \delta_a}$, per deg
$C_{l_{\delta_v}}$	variation of rolling-moment coefficient with rudder deflection, $\dfrac{\partial C_l}{\partial \delta_v}$, per deg

C_m — pitching-moment coefficient, $\dfrac{\text{Pitching moment}}{\bar{q}S\bar{c}}$

$\left(C_{m_q} + C_{m_{\dot{\alpha}}}\right)$ — oscillatory damping-in-pitch derivative, $\left[\dfrac{\partial C_m}{\partial\left(\frac{q\bar{c}}{2V}\right)} + \dfrac{\partial C_m}{\partial\left(\frac{\dot{\alpha}\bar{c}}{2V}\right)}\right]$, per radian

C_{m_α} — longitudinal-stability derivative, $\dfrac{\partial C_m}{\partial\alpha}$, per deg

$\dfrac{C_{m_\alpha}}{C_{N_\alpha}}$ — static margin, fraction of mean aerodynamic chord

$C_{m_{\delta_h}}$ — stabilizer-effectiveness derivative, $\dfrac{\partial C_m}{\partial\delta_h}$, per deg

C_N — normal-force coefficient, $\dfrac{a_n W}{\bar{q}S}$

C_{N_α} — normal-force-curve slope, $\dfrac{\partial C_N}{\partial\alpha}$, per deg

C_n — yawing-moment coefficient, $\dfrac{\text{Yawing moment}}{\bar{q}Sb}$

$\left(C_{n_r} - C_{n_{\dot{\beta}}}\right)$ — oscillatory damping-in-yaw derivative, $\left[\dfrac{\partial C_n}{\partial\left(\frac{rb}{2V}\right)} - \dfrac{\partial C_n}{\partial\left(\frac{\dot{\beta}b}{2V}\right)}\right]$, per radian

C_{n_β} — directional-stability derivative, $\dfrac{\partial C_n}{\partial\beta}$, per deg

$C_{n_{\delta_a}}$ — variation of yawing-moment coefficient with aileron deflection, $\dfrac{\partial C_n}{\partial\delta_a}$, per deg

$C_{n_{\delta_v}}$ — rudder-effectiveness derivative, $\dfrac{\partial C_n}{\partial\delta_v}$, per deg

C_Y — side-force coefficient, $\dfrac{a_t W}{\bar{q}S}$

C_{Y_β} — side-force derivative, $\dfrac{\partial C_Y}{\partial\beta}$, per deg

$\bar{c}$ — mean aerodynamic chord, ft

g	acceleration due to gravity, ft/sec^2
h	geometric altitude, ft
I_X	moment of inertia relative to body X-axis, $slug\text{-}ft^2$
I_Y	moment of inertia relative to body Y-axis, $slug\text{-}ft^2$
I_Z	moment of inertia relative to body Z-axis, $slug\text{-}ft^2$
I_{XZ}	product of inertia, $\frac{1}{2}\left(I_Z - I_X\right)\sin 2\epsilon$, $slug\text{-}ft^2$
M	Mach number
P	period of longitudinal or lateral-directional oscillation, sec
p	rolling angular velocity, radians/sec or deg/sec
q	pitching angular velocity, radians/sec or deg/sec
$\bar{q}$	free-stream dynamic pressure, $\frac{1}{2}\rho V^2$, lb/sq ft
r	yawing angular velocity, radians/sec or deg/sec
S	wing area, sq ft
$T_{1/2}$	time required for transient oscillation to damp to half amplitude, sec
t	time, sec
V	true airspeed, ft/sec
W	airplane weight, lb
α	airplane angle of attack, deg
α_{δ_h}	apparent stability parameter
β	airplane angle of sideslip, deg
δ_a	total aileron deflection (left aileron down positive), $\left(\delta_{h_L} - \delta_{h_R}\right)$, deg
δ_h	horizontal-tail deflection (leading edge up positive), $\frac{1}{2}\left(\delta_{h_L} + \delta_{h_R}\right)$, deg
δ_j	speed-brake deflection, deg

4

δ_v vertical-tail deflection (trailing edge left positive), $\frac{1}{2}\left(\delta_{v_u} + \delta_{v_l}\right)$, deg

ϵ angle of inclination of principal X-axis of airplane relative to the body X-axis (positive when principal X-axis is below body axis at the nose), deg

ζ ratio of actual damping to critical damping

ρ mass density of air, slugs/cu ft

φ roll attitude, deg

Subscripts:

L   left

l lower vertical tail

R   right

u   upper vertical tail

     A dot over a symbol indicates the derivative of the quantity with respect to time. The symbol $|\ \ |$ represents the absolute magnitude of a quantity.

AIRPLANE

     The X-15 airplane (figs. 1 and 2) was designed as a research vehicle to investigate the hypersonic flight regime and is capable of speeds up to about 6,000 feet per second and altitudes greater than 350,000 feet. The cylindrical fuselage is composed mainly of integral propellant tanks, thus requiring fairings on each side of the fuselage to enclose the components of the various systems. A research instrumentation compartment is located immediately to the rear of the cockpit, ahead of the liquid-oxygen tank. Physical characteristics of the airplane are listed in detail in table I.

     For the interim flight program (ref. 1), the X-15 was equipped with two Reaction Motors LR11 rocket engines, installed one above the other in the rear of the fuselage. For the flights to higher Mach numbers, the propulsion unit consists of one Reaction Motors YLR99 variable-thrust, liquid-rocket engine. The YLR99 engine was designed to develop a thrust of 50,000 pounds at sea level, and the ratio of the area of the exhaust to the area of the throat is 9.8. The variation with airplane weight of the moments of inertia of the airplane about the body reference axes for power-on and power-off conditions is shown in figure 3. The center of gravity was approximately 20 percent of the mean aerodynamic chord.

The X-15 has a 5-percent-thick wing with an aspect ratio of 2.5, a 10° wedge-shaped vertical tail, and an all-movable horizontal surface. All aerodynamic control surfaces are positioned by irreversible hydraulic systems. Landing flaps are also hydraulically actuated. The horizontal stabilizer provides longitudinal control when deflected symmetrically and lateral control when deflected differentially. The outer portions of the upper and lower vertical tails are all-moving surfaces affording directional control. Speed brakes are provided at the rear of the inboard sections of the upper and lower vertical tails. Flights are made both with and without the lower rudder. When the lower rudder is on during flight, however, it must be jettisoned before landing to provide adequate ground clearance.

Two of the three X-15 airplanes are equipped with a stability augmentation system (SAS) that provides damping through the aerodynamic-control surfaces to increase three-axes stability. During the flights with the lower rudder on, an interconnect damper system (termed "yar") feeds yaw-rate signals into the roll-control surfaces to provide additional roll damping. The gains and authority of the pitch, roll, yaw, and yar damper systems are shown in table II. The stability augmentation system is discussed in detail in reference 2.

The Honeywell adaptive control system is installed in one of the X-15 airplanes. This system automatically adapts itself to the changing control-surface effectiveness and varying basic-airplane characteristics by providing an essentially constant rate of response to control input.

INSTRUMENTATION

Standard NASA sensing and internal recording instruments, synchronized at 0.1-second intervals by a common timer, were used to record pertinent data, such as normal and transverse accelerations, angular velocities and accelerations, and control-surface deflections.

Airspeed and altitude for the flights with the YLR99 engine were obtained from measurements made by ground-based tracking radar at Edwards, Calif., and at Ely and Beatty, Nev.

Operational limitations did not permit the use of standard NASA free-floating vanes mounted on the nose boom to measure angles of attack and sideslip at Mach numbers beyond 3.4. The sensors were replaced by a gimbal-mounted, null pressure-seeking spherical α and β sensor mounted on the nose of the X-15 (fig. 4). It should be noted that the sensor, or "ball nose," senses the sideslip angle oriented with respect to the stability system of axes; whereas, the angle-of-sideslip vane on the nose boom oriented its reading to the body system of axes. No attempt was made to correct the angle-of-sideslip indications of the ball nose to the body-axes system, inasmuch as the errors in the angle-of-attack range of the flight data were considered to be within the experimental accuracy of the data. For the few data points at an angle of attack of 25°, the error in angle of sideslip is on the order of 10 percent.

The average ranges and dynamic characteristics for the sensing and recording instruments were:

Function	Range	Undamped natural frequency, cps	Damping ratio
α	-20° to 40°	12	0.64
β	±20°	12.5	.64
a_n	-3g to 8g	31	.64
a_t	±1g	18.5	.64
p	[a]±4 radians/sec	[b]18	.62
$\dot{p}$	[c]±6 radians/sec²	[d]18	.62
q	±0.5 radian/sec	12	.62
$\dot{q}$	±1 radian/sec²	12	.62
r	±0.5 radian/sec	12	.62
$\dot{r}$	±1 radian/sec²	12	.62

[a]For X-15-3, ±2 radians/sec.
[b]For X-15-3, 13 cps.
[c]For X-15-3, ±3 radians/sec².
[d]For X-15-3, 13 cps.

Recordings are generally accurate within ±2 percent of the full-scale reading.

FLIGHT-TEST DATA

The derivative characteristics presented in this paper were determined from time histories of pitch, yaw, and roll pulses, random oscillations, and sideslip maneuvers. Most of these maneuvers were performed with either the stability augmentation system or the adaptive control system functioning. Although two dampers were off on several of the maneuvers analyzed, all three dampers were disengaged on only one of the maneuvers. X-15 missions and performance characteristics made it difficult to obtain the type of controlled response at the higher Mach numbers that would lend itself to analysis of both static and dynamic derivatives by use of simplified mathematical expressions. Thus, an analog-matching method (ref. 1) was used to supplement the simple methods of analysis.

A time history of a pitch pulse, representative of those obtained at the higher Mach numbers, is shown in figure 5. Typical time histories of roll and yaw pulses are shown in figures 6 and 7. The roll control was difficult to hold fixed in the lateral-directional maneuvers; therefore, most of the roll- and yaw-pulse maneuvers had some roll-control input during their transient oscillations.

A limited number of sideslip maneuvers were also analyzed to determine static lateral-directional derivatives. A time history of a typical sideslip maneuver is shown in figure 8.

Some random pitch, roll, and yaw oscillations yielded useful data. Figures 9 and 10 are representative time histories of such oscillations.

The maneuvers analyzed covered the following overall ranges of flight conditions: Mach numbers from 0.60 to 6.02; altitudes from 22,400 feet to 131,400 feet; dynamic pressures from 78.5 lb/sq ft to 1,583 lb/sq ft; and angles of attack from -2.7° to 25°. Although the ball-nose readings of angle of attack and angle of sideslip are in error at low subsonic speeds, because of flow effects around the nose of the airplane, all the data presented herein were at low angles of attack where errors are negligible. Figure 11 shows the area in which flight measurements of derivatives were made.

ANALYSIS AND PRESENTATION OF DATA

The mathematical and analog-matching techniques used to obtain the longitudinal and lateral-directional stability and control derivatives of the X-15 airplane at the higher Mach numbers and angles of attack are the same as those used in the study of reference 1. The nature of much of the data precluded the use of simplified mathematical expressions; thus, the analog-matching technique was used to obtain the desired derivatives as well as to verify the results obtained with the simple equations. The results were in good agreement when both methods were used to analyze a particular maneuver which was amenable to the application of the simple equations. Figures 12 and 13 show analog matches of a pitch oscillation and a rudder-induced lateral-directional oscillation, respectively. When the derivatives were obtained by using simplified mathematical expressions, the necessary basic data (periods, time-to-damp to half amplitude, damping ratios, and amplitude ratios) were obtained from time histories similar to that shown in figure 5 for the longitudinal mode and to those shown in figures 6 or 7 for the lateral-directional mode. These basic data are presented in tables III to V. The period is considered accurate within 0.05 second for the low damping ratios ($\zeta < 0.3$).

Often, the augmentation systems could not be completely deactivated because of safety-of-flight restrictions; therefore, the desired controls-fixed condition for many of the pulse maneuvers and oscillations could not be attained. In such instances, an empirical correction to the basic data was applied to account for the effects of the augmentation system (ref. 1).

The longitudinal derivatives C_{N_α}, C_{m_α}, $\dfrac{C_{m_\alpha}}{C_{N_\alpha}}$, $\left(C_{m_q} + C_{m_{\dot{\alpha}}}\right)$, and $C_{m_{\delta_h}}$ are plotted as functions of Mach number and compared with wind-tunnel predictions in figures 14, 15, 16, 17, and 18, respectively. The variation of the lateral-directional derivatives C_{n_β}, C_{l_β}, C_{Y_β}, $\left(C_{n_r} - C_{n_{\dot{\beta}}}\right)$, $C_{n_{\delta_v}}$, $C_{l_{\delta_v}}$, $C_{n_{\delta_a}}$,

and $C_{l_{\delta_a}}$ with Mach number and a comparison with wind-tunnel results are presented in figures 19 to 25. The wind-tunnel data were obtained from the sources listed in references 3 to 16.

DISCUSSION

The derivatives obtained from flight data are discussed in the following sections, and flight-determined characteristics and wind-tunnel predictions are compared. Desired flight data in specific Mach number and angle-of-attack regions were not always obtainable; thus, there are gaps in the derivative presentations over the Mach number range. Trends in the data are generally apparent, however. Although the flight-determined derivatives are presented at various angles of attack within an angle-of-attack range, the wind-tunnel data are given only for the average angle of attack of the flight-test range. Comparison of the flight-determined and the wind-tunnel derivatives shows the correlation between the data. No attempt was made to correlate the flight-determined derivatives with the results of theoretical studies; this comparison may be found in reference 17.

Longitudinal Derivatives

In the flight data presented in figures 14 to 18, the longitudinal stability and control derivatives show the usual trends of increasing levels of lift-curve slope, static stability, damping, and control effectiveness through the transonic region and diminishing levels of these characteristics as Mach number increases in the supersonic region. Although a distinction between power-on and power-off conditions is made in the flight data, power effects do not appear to be significant. No distinction has been made between lower-rudder-on and lower-rudder-off data because the rudder has little effect on the longitudinal characteristics. The effect of speed brakes is shown only for C_{m_α}, inasmuch as the other longitudinal derivatives are not significantly influenced by speed-brake deployment. Insufficient longitudinal data were obtained with the speed brakes open to enable any conclusions to be made on the effects of the brakes.

The peak value of the stability derivative C_{m_α} (fig. 15) occurs at a slightly higher Mach number than the control-effectiveness derivative $C_{m_{\delta_h}}$ (fig. 18) and at low supersonic speeds decreases more slowly than $C_{m_{\delta_h}}$ with increasing Mach number. These trends result in a general decrease in the apparent stability parameter α_{δ_h}, obtained from $\dfrac{C_{m_{\delta_h}}}{C_{m_\alpha}}$, as speed increases from subsonic Mach numbers to $M \approx 2.5$, followed by some indication of an increase in apparent stability at higher speeds. An appreciable level of longitudinal stability is indicated by the static margin obtained from $\dfrac{C_{m_\alpha}}{C_{N_\alpha}}$ (fig. 16),

9

particularly for low supersonic speeds. The damping derivative $\left(C_{m_q} + C_{m_{\dot{\alpha}}}\right)$ (fig. 17), which is moderately high in the transonic region, decreases rapidly between Mach numbers of 1 and 2 and remains at a relatively constant level above $M = 2.0$.

In general, the longitudinal flight and wind-tunnel data are in fairly good agreement, with the flight data indicating that the predicted levels of stability have been realized. At angles of attack up to 6°, the flight-determined static-stability derivative C_{m_α} is slightly higher than anticipated between $M = 1.3$ and $M = 2.0$ (fig. 15). In the lower range of stabilizer positions, the values of $C_{m_{\delta_h}}$ obtained from flight data are slightly lower than those predicted by wind-tunnel tests (fig. 18). Although the damping derivative $\left(C_{m_q} + C_{m_{\dot{\alpha}}}\right)$ is more difficult to obtain than the static derivatives, because of inadvertent control inputs, the flight-determined values of this derivative are in good agreement with wind-tunnel data.

Lateral-Directional Derivatives

Fairly good consistency is shown in the variation of the flight-determined lateral-directional stability and control derivatives with Mach number (figs. 19 to 25). Both power-on and power-off data are presented, but no specific power effect is noted.

In the low-angle-of-attack region, the static directional-stability derivative C_{n_β} (fig. 19(a)) peaks at about $M = 1.3$ then diminishes rapidly until $M \approx 2.5$. Above $M \approx 2.5$ the rate of decrease is much lower. At Mach numbers below approximately 2, the value of C_{n_β} decreases substantially as the angle of attack increases. At high Mach numbers the increase in effectiveness of the lower vertical tail with increasing angle of attack, as a result of the high intensity of the bow and wing compression shocks, more than offsets the decrease in effectiveness of the upper vertical tail, which is in the expansion field. The result is that C_{n_β} increases with increasing angle of attack (ref. 17).

When the lower rudder is removed, the anticipated decrease in the value of C_{n_β} is evident (fig. 19(b)), with as much as a 50-percent drop noted for Mach numbers above 3.0 at low angles of attack. The negligible values of C_{n_β} between $M = 3.0$ and 3.5 at moderate angles of attack indicate that the vertical tail with the lower rudder off barely compensates for wing-fuselage instability in this flight range.

In general, there is a favorable increment in C_{n_β} when the speed brakes are open. This increment decreases as angle of attack increases.

With the lower rudder on, there is a positive trend in the flight data for the effective dihedral derivative C_{l_β} in all angle-of-attack areas as the Mach

10

number increases (fig. 20(a)). The values of this derivative change from favorable (negative) to adverse near $M = 2.2$ and change little with increase in Mach number above $M = 3.0$. This positive trend is caused by the asymmetry in effectiveness between the upper and lower vertical tails resulting from bow and wing shock expansion and compression fields (ref. 17). The adverse dihedral effect at higher Mach numbers is relieved when the lower rudder is removed, as shown in figure 20(b) where the values of C_{l_β} determined from flight maneuvers with the lower rudder off are favorable for the Mach number and angle-of-attack range studied. There seems to be little effect of speed-brake deployment on C_{l_β} at low angles of attack; however, C_{l_β} is generally more adverse with speed brakes open at the higher angles of attack.

With the lower rudder on, the values of the side-force derivative C_{Y_β} (fig. 21(a)) increase to the transonic region, then gradually decrease with rising Mach number. With the lower rudder removed (fig. 21(b)), the values of the side-force derivative are appreciably lower in all Mach number and angle-of-attack ranges investigated. At the low angles of attack, speed-brake deployment raises, in general, the level of C_{Y_β}.

The flight-determined values of the damping-in-yaw derivative $\left(C_{n_r} - C_{n_{\dot\beta}}\right)$ for the lower-rudder-on configuration peak in the transonic region, then show a gradual decline with increasing Mach number (fig. 22). Within the accuracy of the data, there seems to be little angle-of-attack effect. The scatter in the SAS-on data is probably due to the large SAS corrections for damping-in-yaw derivatives, which give rise to considerable uncertainty in the flight data (ref. 1). Too little damping-in-yaw data have been obtained with the lower rudder off to be considered in this paper.

The flight control derivatives are characterized by peak magnitudes in the transonic range and decreasing levels with increasing Mach number (figs. 23 to 25). The data for lower-rudder-on and lower-rudder-off configurations of the airplane are presented separately for values of $C_{n_{\delta_v}}$ and $C_{l_{\delta_v}}$ but are combined for $C_{l_{\delta_a}}$ and $C_{n_{\delta_a}}$, since there is no discernible difference in the data for the latter two derivatives with the two tail configurations.

The value of the flight-determined directional-control derivative $C_{n_{\delta_v}}$, similar to C_{n_β}, decreases considerably when the lower rudder is removed (fig. 23(b)). Moreover, $C_{n_{\delta_v}}$ shows no significant angle-of-attack effect with the lower rudder on (fig. 23(a)), but decreases appreciably with increase in angle of attack when the lower rudder is removed.

When the lower rudder is on, $C_{l_{\delta_v}}$ changes from positive to negative as Mach number increases in the supersonic range (fig. 24(a)). This sign reversal occurs at a lower Mach number at the higher angles of attack than at the lower angles of attack. When the lower rudder is off (fig. 24(b)), $C_{l_{\delta_v}}$ remains

positive throughout the Mach number and angle-of-attack ranges studied. With the lower rudder on, $C_{l_{\delta_v}}$ becomes more negative with increasing angle of attack. With the lower rudder off, $C_{l_{\delta_v}}$ becomes less positive with increasing angle of attack.

Some scatter is noted in both the $C_{n_{\delta_a}}$ and $C_{l_{\delta_a}}$ flight data (fig. 25), particularly at the high angles of attack; this scatter is partly the result of differences in angle of attack within the 12° to 24° range. For Mach numbers greater than 4, the flight values of both $C_{n_{\delta_a}}$ and $C_{l_{\delta_a}}$ are generally higher at the larger angles of attack than at the smaller values.

In general, the flight data for C_{n_β} (fig. 19) confirm the wind-tunnel predictions, although there is a somewhat lower level in the flight values of C_{n_β} with the lower rudder on at low angles of attack and at supersonic Mach numbers. Also, a smaller increment in the flight-determined values of C_{n_β} resulting from speed-brake deployment at moderate and large angles of attack is apparent, and the flight data show an appreciable scatter in the C_{n_β} increment as a result of speed-brake deflection. The flight-determined dihedral derivatives are also generally in accord with the wind-tunnel measurements. The variation with Mach number of the side-force derivatives determined from flight data shows good correlation with wind-tunnel data at all angles of attack when the lower rudder is on and at low angles of attack when the lower rudder is off. The scarcity of flight data at the higher angles of attack for the lower-rudder-off configuration precludes any valid comparison. The values of the damping derivative $\left(C_{n_r} - C_{n_{\dot\beta}}\right)$ determined in flight agree, in general, with the wind-tunnel predictions, although the flight data show considerable scatter when the stability augmentation system is engaged. When the lower rudder is on, values of $C_{n_{\delta_v}}$ obtained from flight data are slightly lower than predicted by wind-tunnel tests. This lower trend appears to coincide with the aforementioned lower level of the flight-determined stability derivative. Lower levels in the flight-determined derivatives are also apparent for $C_{n_{\delta_a}}$ and $C_{l_{\delta_a}}$ in the hypersonic region. Except as noted, all flight-determined control parameters show fairly good agreement with the wind-tunnel results.

CONCLUSIONS

Flight tests of the X-15 airplane to determine stability and control derivatives to a Mach number of 6.02 and an angle of attack of 25° with speed brakes open and closed, lower rudder on and off, and power on and off indicate the following:

1. The longitudinal stability and control derivatives showed the usual trends of increasing levels through the transonic region and diminishing levels as Mach number increased in the supersonic region. A relatively high level of

12

longitudinal stability was indicated by the static-margin parameter $\dfrac{C_{m_\alpha}}{C_{N_\alpha}}$, particularly for low supersonic speeds. The damping derivative $\left(C_{m_q} + C_{m_{\dot\alpha}}\right)$ decreased rapidly between Mach numbers of 1 and 2, then remained fairly constant for higher Mach numbers.

2. With the lower rudder on, the values of the lateral-directional derivatives, except C_{l_β}, in the low and moderate angle-of-attack ranges increased to the transonic region and then declined with rising Mach number. At the higher Mach numbers, the directional-stability derivative C_{n_β} increased with increasing angle of attack. The effective dihedral derivative C_{l_β} had a positive trend as the Mach number increased and changed from favorable to adverse near a Mach number of 2.2.

3. When the lower rudder was removed, the value of the static directional-stability derivative C_{n_β} dropped as much as 50 percent above a Mach number of 3.0 at low angles of attack. At moderate angles of attack the value of C_{n_β} approached zero near a Mach number of 3.5. A decided decrease in the levels of the side-force derivative C_{Y_β} and the rudder-effectiveness derivative $C_{n_{\delta_V}}$ also occurred with the removal of the lower rudder. However, when the lower rudder was removed, the values of the effective dihedral C_{l_β} remained favorable (negative) and the values of the cross-control derivative $C_{l_{\delta_V}}$ remained positive for the Mach number and angle-of-attack ranges investigated.

4. Opening the speed brakes produced favorable increments in the values of both C_{n_β} and C_{Y_β}; however, the C_{n_β} increment decreased as the angle of attack increased. On the whole, little effect of speed-brake deployment on the effective dihedral derivative C_{l_β} was apparent at low angles of attack, but the derivative appeared to be somewhat more adverse with speed brakes open at the higher angles of attack.

5. Although both power-on and power-off conditions were investigated, there appears to be no specific power effect on the trend of any of the principal derivatives.

6. The flight-determined derivatives are, with a few exceptions, in agreement with the wind-tunnel predictions. The static longitudinal-stability derivative C_{m_α} determined from flight data is slightly higher than predicted by wind-tunnel tests at low angles of attack in the Mach number range from 1.3 to 2.0. The flight-determined directional-stability derivative C_{n_β} and the vertical-tail-effectiveness derivative $C_{n_{\delta_V}}$ show slightly lower values at low angles of attack and at supersonic Mach numbers than do the wind-tunnel data at

the same conditions. A trend to values lower than predicted is also evident in the hypersonic regions for the flight-determined roll-control derivative $C_{l_{\delta_a}}$.

Flight Research Center,
        National Aeronautics and Space Administration,
                Edwards, Calif., July 13, 1964.

14

REFERENCES

1. Yancey, Roxanah B., Rediess, Herman A., and Robinson, Glenn H.: Aerodynamic-Derivative Characteristics of the X-15 Research Airplane as Determined From Flight Tests for Mach Numbers From 0.6 to 3.4. NASA TN D-1060, 1962.

2. Tremant, Robert A.: Operational Experiences and Characteristics of the X-15 Flight Control System. NASA TN D-1402, 1962.

3. Anon: Revised Basic Aerodynamic Characteristics of the X-15 Research Airplane. Rep. NA-59-1203, (Contract AF 33(600)-31693), North American Aviation, Inc., Aug. 7, 1959.

4. Hassell, James L., Jr., and Hewes, Donald E.: Investigation of the Subsonic Stability and Control Characteristics of the 1/7-Scale Model of the North American X-15 Airplane With and Without Fuselage Forebody Strakes. NASA TM X-210, 1960.

5. Lopez, Armando E., and Tinling, Bruce E.: The Static and Dynamic-Rotary Stability Derivatives at Subsonic Speeds of a Model of the X-15 Research Airplane. NASA RM A58F09, 1958.

6. Driver, Cornelius: Effect of Forebody Strakes on the Aerodynamic Characteristics in Pitch and Sideslip of a Hypersonic Airplane Configuration at Mach Numbers of 1.41, 2.01, and 6.86. NASA TM X-116, 1959.

7. Tunnell, Phillips J., and Latham, Eldon A.: The Static and Dynamic-Rotary Stability Derivatives of a Model of the X-15 Research Airplane at Mach Numbers From 1.55 to 3.50. NASA MEMO 12-23-58A, 1959.

8. Franklin, Arthur E., and Lust, Robert M.: Investigation of the Aerodynamic Characteristics of a 0.067-Scale Model of the X-15 Airplane (Configuration 3) at Mach Numbers of 2.29, 2.98, and 4.65. NASA TM X-38, 1959.

9. Anon: A Third Series of Supersonic Force Tests on the Full-Span Model X-15 for North American Aviation, Inc. WTR 228, M.I.T. Naval Supersonic Lab., Nov. 1958.

10. Anon: A Fourth Series of Supersonic Force Tests on the Full-Span Model X-15 for North American Aviation, Incorporated. WTR 239, M.I.T. Naval Supersonic Lab., Dec. 1958.

11. Dunning, Robert W.: The Control Characteristics of Two Preliminary Models of the X-15 Research Airplane at Mach Numbers of 2.98 and 4.01. NASA TM X-212, 1960.

12. Penland, Jim A., and Fetterman, David E., Jr.: Static Longitudinal, Directional, and Lateral Stability and Control Data at a Mach Number of 6.83 of the Final Configuration of the X-15 Research Airplane. NASA TM X-236, 1960.

13. Paulson, John W., and Hassell, James L., Jr.: Low-Speed Measurements of Oscillatory Lateral Stability Derivatives of a 1/7-Scale Model of the North American X-15 Airplane. NASA TM X-144, 1959.

14. McKinney, Royce L., and Lancaster, Julia A.: Investigation of the Aerodynamic Characteristics of a 0.02-Scale Model of the X-15 Airplane at Mach Numbers of 2.96, 3.96, and 4.65 at High Angles of Attack. NASA TM X-820, 1963.

15. Nelson, Duane A.: Test of a 0.02-Scale Model of the North American Aviation X-15 in the 21-Inch Hypersonic Wind Tunnel. WT 21-32, Jet Prop. Lab., C.I.T., Mar. 3, 1961.

16. Nelson, Duane A.: Test of a 0.02-Scale Model of the North American Aviation X-15. WT 21-63, Jet Prop. Lab., C.I.T., Mar. 21, 1962.

17. Walker, Harold J., and Wolowicz, Chester H.: Stability and Control Derivative Characteristics of the X-15 Airplane. NASA TM X-714, 1962.

TABLE I.- PHYSICAL CHARACTERISTICS OF THE X-15 AIRPLANE

Wing:
```
Airfoil section . . . . . . . . . . . . . . . . . . . . . . . NACA 66005 (modified)
Total area (includes 94.98 sq ft covered by
    fuselage), sq ft . . . . . . . . . . . . . . . . . . . . . . .        200
Span, ft . . . . . . . . . . . . . . . . . . . . . . . . . . . .        22.36
Mean aerodynamic chord, ft . . . . . . . . . . . . . . . . . .        10.27
Root chord, ft . . . . . . . . . . . . . . . . . . . . . . . .        14.91
Tip chord, ft . . . . . . . . . . . . . . . . . . . . . . . . .         2.98
Taper ratio . . . . . . . . . . . . . . . . . . . . . . . . . .         0.20
Aspect ratio . . . . . . . . . . . . . . . . . . . . . . . . .          2.50
Sweep at 25-percent chord line, deg . . . . . . . . . . . . . .        25.64
Incidence, deg . . . . . . . . . . . . . . . . . . . . . . . .            0
Dihedral, deg . . . . . . . . . . . . . . . . . . . . . . . . .           0
Aerodynamic twist, deg . . . . . . . . . . . . . . . . . . . .            0
Flap -
    Type . . . . . . . . . . . . . . . . . . . . . . . . . . . .        Plain
    Area (each), sq ft . . . . . . . . . . . . . . . . . . . .           8.30
    Span (each), ft . . . . . . . . . . . . . . . . . . . . . .          4.50
    Inboard chord, ft . . . . . . . . . . . . . . . . . . . . .          2.61
    Outboard chord, ft . . . . . . . . . . . . . . . . . . . . .         1.08
    Deflection, maximum down, deg . . . . . . . . . . . . . . .           40
    Ratio flap chord to wing chord . . . . . . . . . . . . . . .         0.22
    Ratio total flap area to wing area . . . . . . . . . . . . .        0.08
    Ratio flap span to wing semispan . . . . . . . . . . . . . .        0.40
    Trailing-edge angle, deg . . . . . . . . . . . . . . . . . .         5.67
    Sweepback angle of hinge line, deg . . . . . . . . . . . . .           0
```

Horizontal tail:
```
Airfoil section . . . . . . . . . . . . . . . . . . . . . . . NACA 66005 (modified)
Total area (includes 63.29 sq ft covered by
    fuselage), sq ft . . . . . . . . . . . . . . . . . . . . . .        115.34
Span, ft . . . . . . . . . . . . . . . . . . . . . . . . . . . .        18.08
Mean aerodynamic chord, ft . . . . . . . . . . . . . . . . . .         7.05
Root chord, ft . . . . . . . . . . . . . . . . . . . . . . . .        10.22
Tip chord, ft . . . . . . . . . . . . . . . . . . . . . . . . .         2.11
Taper ratio . . . . . . . . . . . . . . . . . . . . . . . . . .         0.21
Aspect ratio . . . . . . . . . . . . . . . . . . . . . . . . .          2.83
Sweep at 25-percent chord line, deg . . . . . . . . . . . . . .           45
Dihedral, deg . . . . . . . . . . . . . . . . . . . . . . . . .          -15
Ratio horizontal-tail area to wing area . . . . . . . . . . . .         0.58
Movable-surface area, sq ft . . . . . . . . . . . . . . . . . .        51.77
Deflection -
    Longitudinal, up, deg . . . . . . . . . . . . . . . . . . . .          15
    Longitudinal, down, deg . . . . . . . . . . . . . . . . . . .          35
    Lateral differential (pilot authority), deg . . . . . . . . .        ±15
    Lateral differential (autopilot authority), deg . . . . . . .        ±30
Control system . . . . . . . . Irreversible hydraulic boost with artificial feel
```

TABLE I.- PHYSICAL CHARACTERISTICS OF THE X-15 AIRPLANE (Concluded)

Upper vertical tail:
  Airfoil section . . . . 10° single wedge
  Total area, sq ft 40.91
  Span, ft 4.58
  Mean aerodynamic chord, ft 8.95
  Root chord, ft 10.21
  Tip chord, ft 7.56
  Taper ratio 0.74
  Aspect ratio 0.51
  Sweep at 25-percent chord line, deg 23.41
  Ratio vertical-tail area to wing area 0.20
  Movable-surface area, sq ft 26.45
  Deflection, deg . . . . ±7.50
  Sweepback of hinge line, deg 0
  Control system . . . . Irreversible hydraulic boost with artificial feel

Lower vertical tail:
  Airfoil section . . . . 10° single wedge
  Total area, sq ft 34.41
  Span, ft 3.83
  Mean aerodynamic chord, ft 9.17
  Root chord, ft 10.21
  Tip chord, ft 8
  Taper ratio 0.78
  Aspect ratio 0.43
  Sweep at 25-percent chord line, deg 23.41
  Ratio vertical-tail area to wing area 0.17
  Movable-surface area, sq ft 19.95
  Deflection, deg . . . . ±7.50
  Sweepback of hinge line, deg 0
  Control system . . . . Irreversible hydraulic boost with artificial feel

Fuselage:
  Length, ft 50.75
  Maximum width, ft 7.33
  Maximum depth, ft 4.67
  Maximum depth over canopy, ft 4.97
  Side area (total), sq ft 215.66
  Fineness ratio 10.91

Speed brake (typical for each of four):
  Area, sq ft 5.57
  Span, ft 1.67
  Chord, ft 3.33
  Deflection, deg 35

Center-of-gravity location, percent mean aerodynamic chord . . . . 20 ±1

                                                            Launch   Landing
Weight, lb 33,000   14,700

18

TABLE II.- GAIN AND AUTHORITY OF THE X-15 STABILITY AUGMENTATION SYSTEM

	Gain							
Switch position	Pitch		Roll		Yaw		Yar	
	In./deg/sec	Deg/deg/sec	In./deg/sec	Deg/deg/sec	In./deg/sec	Deg/deg/sec	In./deg/sec	Deg/deg/sec
1	0.005	0.075	0.0017	0.051	0.004	0.03	0.003	0.09
2	.010	.150	.0033	.100	.008	.06	.006	.18
3	.015	.225	.0050	.150	.012	.09	.009	.27
4	.020	.300	.0067	.200	.016	.12	.012	.36
5	.025	.375	.0083	.250	.020	.15	.015	.45
6	.030	.450	.0100	.300	.024	.18	.018	.54
7	.035	.525	.0117	.350	.028	.21	.021	.63
8	.040	.600	.0134	.400	.032	.24	.024	.72
9	.045	.675	.0150	.450	.036	.27	.027	.81
10	.050	.750	.0167	.500	.040	.30	.030	.90

Condition	Servo and surface limits			
Normal functioning	Maximum servo-actuator travel = ±1.0 inch or ±15° of horizontal stabilizer	Maximum servo-actuator travel = ±1.0 inch or ±15° of horizontal stabilizer	Maximum servo-actuator travel = ±1.0 inch or ±7.5° of vertical stabilizer	Maximum servo-actuator travel = ±1.0 inch or ±15° of horizontal stabilizer
Mal-functioning	0.1 inch or 1.5° of horizontal stabilizer	0.1 inch or 3° differential stabilizer	0.1 inch or 0.75° of vertical stabilizer	0.1 inch or 3° of differential stabilizer

TABLE III.- BASIC DATA FOR LONGITUDINAL MANEUVERS

M	α, deg	q̄, lb/sq ft	h, ft	aₙ, g	Power	Speed brakes	SAS gain setting (a)	$\frac{|a_n|}{|\alpha|}$	$\frac{|q|}{|\alpha|}$	P, sec	$T_{1/2}$, sec	ζ
1.10	9.6	268.0	47,100	2.29	Off	Closed	8,6,8	----	----	1.00	----	----
1.17	7.6	325.0	45,100	.75	On	Closed	0,8,8	----	----	1.90	2.25	0.093
1.28	7.7	172.5	60,200	1.13	Off	Closed	0,4,8	10.11	2.21	2.36	4.36	.060
1.41	14.1	176.0	63,625	1.50	Off	Closed	F,F,F	9.26	4.64	2.03	1.72	.129
1.47	6.7	235.0	60,225	.86	Off	Open	A,A,A	14.19	3.64	1.30	1.26	.113
1.82	6.5	305.0	63,625	1.23	Off	Open	F,F,F	14.80	----	1.50	1.90	.087
1.95	3.9	955.0	43,200	1.33	On	Closed	0,8,8	----	----	1.10	∞	----
2.14	5.2	1187.5	42,000	2.50	On	Closed	0,8,8	----	----	1.00	∞	----
2.46	4.6	1583.0	41,900	2.50	On	Closed	0,7,8	----	----	1.00	∞	----
2.46	7.4	369.0	70,800	1.10	Off	Open	F,F,F	15.04	3.98	1.50	2.10	.078
2.90	3.2	1490.0	50,000	1.60	On	Closed	0,7,8	----	----	1.08	∞	----
3.30	7.4	420.0	80,675	.93	Off	Open	F,F,F	12.43	3.31	1.90	6.74	.031
3.41	-2.7	1218.0	61,000	.85	On	Closed	0,7,8	21.88	3.94	1.40	2.50	.062
4.00	8.9	189.0	107,050	.47	Off	Closed	0,4,8	14.70	1.10	4.66	9.00	.056
4.20	3.3	253.0	102,500	.42	Off	Closed	0,4,8	4.08	1.32	3.60	3.75	.105
4.34	2.1	494.4	88,450	.04	Off	Closed	4,4,6	----	----	2.30	1.73	.145
4.36	1.0	331.5	98,450	.08	Off	Closed	0,4,8	5.96	1.80	3.00	12.00	.034
4.37	-.3	941.0	76,250	-.05	On	Closed	0,7,8	----	----	2.00	∞	----
4.40	2.2	355.0	97,400	.22	Off	Closed	0,4,8	7.78	2.12	2.70	3.70	.080
4.49	2.5	412.5	95,100	.26	Off	Closed	0,4,4	8.53	1.68	2.90	7.30	.044
4.57	2.2	788.3	79,450	.12	Off	Closed	4,4,6	----	----	2.10	∞	----
4.59	2.2	493.0	92,050	.40	Off	Closed	0,4,4	----	----	2.60	∞	----
5.10	6.0	745.0	87,200	1.90	Off	Open	8,0,0	16.88	----	1.90	1.34	.154
5.44	3.3	592.0	95,100	.50	Off	Open	8,0,0	13.06	----	1.80	2.44	.081

ᵃNumbers for SAS settings are damper-gain knob positions for pitch, roll, and yaw, respectively. Damper gains corresponding to various knob settings are shown in table II. The letters A and F denote adaptive control and fixed gain, respectively.

TABLE IV.- BASIC DATA FOR LATERAL-DIRECTIONAL MANEUVERS

[LOWER RUDDER ON]

M	α, deg	$\bar{q}$, lb/sq ft	h, ft	Power	Speed brakes	SAS gain setting (a)	$\dfrac{|r|}{|\beta|}$	$\dfrac{|a_t|}{|\beta|}$	P, sec	$T_{1/2}$, sec	ζ
0.87	2.7	503.0	63,475	Off	Open	8,6,8	3.88	8.18	1.60	0.87	0.199
1.62	7.3	492.0	48,400	On	Closed	0,0,0	3.10	7.05	1.60	1.58	.111
1.62	10.6	224.5	64,450	Off	Closed	4,4,6	----	----	1.60	1.20	.146
2.44	2.6	554.0	61,805	Off	Open	8,6,8	4.13	8.99	1.50	1.40	.117
2.47	8.7	517.5	65,775	Off	Open	8,8,0	----	9.35	2.10	4.48	.052
2.58	6.4	544.5	66,800	Off	Open	8,0,0	3.42	7.01	2.20	∞	-----
2.68	7.4	483.0	71,150	Off	Open	8,6,0	3.27	8.57	2.26	8.60	.029
2.74	5.0	571.5	68,400	Off	Open	8,0,0	3.62	7.18	2.05	5.35	.042
2.84	1.8	545.8	69,398	Off	Open	4,4,4	4.16	.17	1.60	1.39	.126
2.97	1.7	514.3	72,457	Off	Open	4,4,4	3.92	.15	1.68	1.40	.131
2.99	2.0	466.0	77,054	On	Closed	8,6,8	2.17	3.93	2.60	1.36	.206
3.04	7.4	473.0	76,775	Off	Open	8,6,8	3.70	8.00	2.50	11.30	.025
3.11	1.7	501.3	74,938	Off	Open	4,4,4	3.87	.13	1.68	1.85	.099
3.40	4.5	653.5	74,450	Off	Open	8,0,0	3.86	7.80	2.00	∞	-----
3.40	7.3	467.5	80,850	Off	Closed	8,6,8	3.03	----	3.00	1.37	.234
3.41	2.6	506.0	79,350	Off	Open	8,6,8	3.75	9.79	1.78	4.75	.041
3.46	9.8	439.0	83,050	Off	Closed	8,6,8	----	----	3.40	1.20	.298
3.50	7.7	280.0	92,250	Off	Closed	0,4,8	2.26	----	3.30	5.20	.215
3.54	8.7	449.5	84,400	Off	Open	8,8,0	----	8.46	2.70	-6.50	-.046
3.61	6.8	717.1	73,648	Off	Closed	4,4,4	3.25	.16	2.50	1.78	.153
3.70	12.5	260.0	97,325	Off	Closed	8,6,8	2.46	4.17	4.20	2.47	.184
3.84	8.1	302.2	96,350	Off	Open	6,6,0	2.84	5.89	2.60	-32.30	-.009
3.84	8.2	342.0	93,525	Off	Closed	8,6,8	2.34	5.71	3.60	3.70	.107
3.99	11.4	226.0	104,200	Off	Closed	8,6,8	1.99	3.05	6.00	4.35	.150
4.08	2.6	796.3	76,618	Off	Closed	4,4,4	4.25	.20	2.00	2.63	.084
4.14	9.7	330.0	97,675	Off	Closed	8,6,8	2.76	5.25	3.60	4.50	.109
4.31	12.8	238.8	106,650	Off	Closed	8,6,8	----	----	5.00	-----	-----
4.32	8.0	321.0	99,000	Off	Open	8,6,8	2.85	5.69	2.60	2.15	.132
4.33	2.9	892.8	76,741	Off	Closed	4,4,4	3.45	.18	2.10	1.43	.160
4.36	10.5	318.0	100,450	Off	Closed	8,6,8	2.43	5.56	4.20	9.50	.049
4.40	2.2	355.0	97,400	Off	Closed	0,4,4	2.05	5.18	3.00	7.30	.045
4.43	2.0	558.5	86,000	Off	Closed	4,4,6	----	----	2.30	1.67	.102
4.48	12.4	256.0	106,800	Off	Closed	4,4,8	1.95	----	4.40	4.38	.110
4.76	10.8	281.2	107,625	Off	Closed	8,6,8	1.96	----	5.00	6.15	.089
4.87	25.1	203.2	115,350	Off	Open	A,A,F	4.67	5.05	2.45	-4.25	-.063
5.10	.7	396.0	102,875	Off	Closed	8,6,8	2.02	----	2.80	1.24	.242
5.18	.6	458.0	99,900	Off	Closed	8,6,8	2.29	----	2.80	2.18	.140
5.47	3.1	573.0	96,250	Off	Open	8,0,0	3.62	8.72	1.72	∞	-----
5.55	2.7	478.0	101,550	Off	Open	8,0,0	3.05	7.84	2.00	∞	-----
5.59	1.7	485.0	100,725	Off	Closed	8,0,0	1.89	5.33	3.20	∞	-----
5.62	1.6	482.0	101,400	Off	Closed	8,0,0	1.81	5.45	3.40	∞	-----

aNumbers for SAS gain settings are damper-gain knob positions for pitch, roll, and yaw, respectively. Damper gains corresponding to various knob settings are shown in table II. The letters A and F denote adaptive control and fixed gain, respectively.

TABLE V.- BASIC DATA FOR LATERAL-DIRECTIONAL MANEUVERS

[LOWER RUDDER OFF]

M	α, deg	$\bar{q}$, lb/sq ft	h, ft	Power	Speed brakes	SAS gain setting (a)	$\dfrac{\lvert r\rvert}{\lvert\beta\rvert}$	$\dfrac{\lvert a_t\rvert}{\lvert\beta\rvert}$	P, sec	$T_{1/2}$, sec	ζ
0.82	7.4	246.0	35,000	Off	Closed	A,0,0	1.02	3.25	2.50	2.54	0.108
.87	6.6	219.0	36,100	Off	Closed	A,0,0	1.38	3.66	2.40	2.36	.112
1.04	5.3	257.5	44,450	Off	Closed	8,4,4	1.92	---	2.60	3.00	.095
1.06	3.9	319.0	40,600	Off	Closed	A,0,0	1.27	4.97	2.25	2.00	.123
1.14	3.6	283.0	46,100	Off	Closed	8,4,4	2.30	4.45	2.50	2.36	.116
1.59	3.4	490.0	48,600	Off	Closed	8,4,4	3.20	---	1.80	1.25	.157
1.75	4.2	583.0	49,350	Off	Closed	8,4,4	3.03	8.10	1.80	1.28	.153
2.19	3.4	516.0	60,600	Off	Open	8,4,4	1.99	6.78	2.60	2.30	.124
2.26	10.0	288.0	74,825	Off	Closed	8,0,0	.80	3.54	3.37	3.32	.111
2.33	4.8	326.0	72,010	Off	Closed	A,0,0	1.30	4.75	3.00	5.00	.066
2.34	2.1	207.0	81,475	Off	Closed	A,0,0	1.20	3.78	4.20	4.80	.096
2.34	3.7	240.0	78,575	Off	Open	A,0,0	1.32	3.32	3.70	10.20	.040
2.45	2.6	937.0	52,950	Off	Open	A,F,F	2.30	13.98	1.64	.86	.210
2.46	.7	376.0	71,600	Off	Open	8,0,4	2.56	6.28	2.40	2.50	.105
2.46	3.0	767.0	57,900	Off	Open	A,0,0	2.93	12.17	1.65	3.10	.059
2.62	2.5	832.5	58,275	Off	Closed	A,F,F	1.90	9.70	1.99	1.45	.150
2.75	2.2	842.5	60,350	Off	Open	A,F,F	2.40	11.89	1.60	1.52	.116
2.77	6.6	530.0	68,800	Off	Open	8,0,4	1.43	---	2.10	2.24	.103
2.78	-2.3	391.5	76,050	On	Open	8,4,4	3.21	4.32	2.10	8	---
2.84	3.1	679.0	65,450	On	Open	A,F,F	1.50	10.60	1.95	1.17	.181
2.84	3.7	376.5	78,700	Off	Closed	8,0,0	1.09	4.08	3.60	5.77	.069
3.11	10.4	431.8	80,175	Off	Closed	8,0,0	.35	4.02	3.00	3.90	.085
3.45	10.7	418.5	84,600	Off	Closed	8,0,0	.33	4.40	3.80	3.67	.114
3.71	9.9	301.5	95,900	Off	Open	8,0,4		---	3.50		---
3.74	2.0	929.0	70,425	Off	Open	8,0,0	2.87	13.90	1.80	2.40	.082
3.78	4.0	226.2	101,775	Off	Open	8,0,0	1.63	3.24	3.00	19.80	.017
3.84	3.9	227.2	103,750	Off	Open	8,0,0	1.49	2.69	3.20	12.20	.024
3.91	3.7	237.0	103,475	Off	Open	8,0,0	1.71	2.79	3.40	9.80	.038
4.07	3.8	898.0	74,600	On	Open	8,4,4	3.28	---	1.80	1.65	.119
4.59	8.7	687.5	86,150	Off	Open	A,0,0	2.13	8.90	2.30	12.00	.021
4.66	7.7	624.5	87,800	Off	Closed	A,F,0	.63	6.19	4.60	1.67	.129
4.83	16.5	592.5	92,250	Off	Open	8,0,0	1.91	8.50	2.48	8.80	.031
4.88	5.2	889.0	83,600	Off	Open	A,F,0	2.12	13.50	2.00	3.75	.059
4.96	6.4	372.0	101,500	Off	Closed	8,0,0	.54	3.42	3.05	6.96	.048
4.98	5.2	364.0	102,250	Off	Closed	A,F,0	.72	4.44	5.20	5.05	.113
5.26	5.3	559.0	97,550	Off	Open	8,0,0	1.48	5.59	2.50	4.95	.056
5.37	4.6	309.5	111,750	Off	Closed	8,4,8	.89	2.83	5.00	8.10	.069

aNumbers for SAS gain settings are damper-gain knob positions for pitch, roll, and yaw, respectively. Damper gains corresponding to various knob settings are shown in table II. The letters A and F denote adaptive control and fixed gain, respectively.

Fuselage reference line

49.17

39.1

18.08

22.36
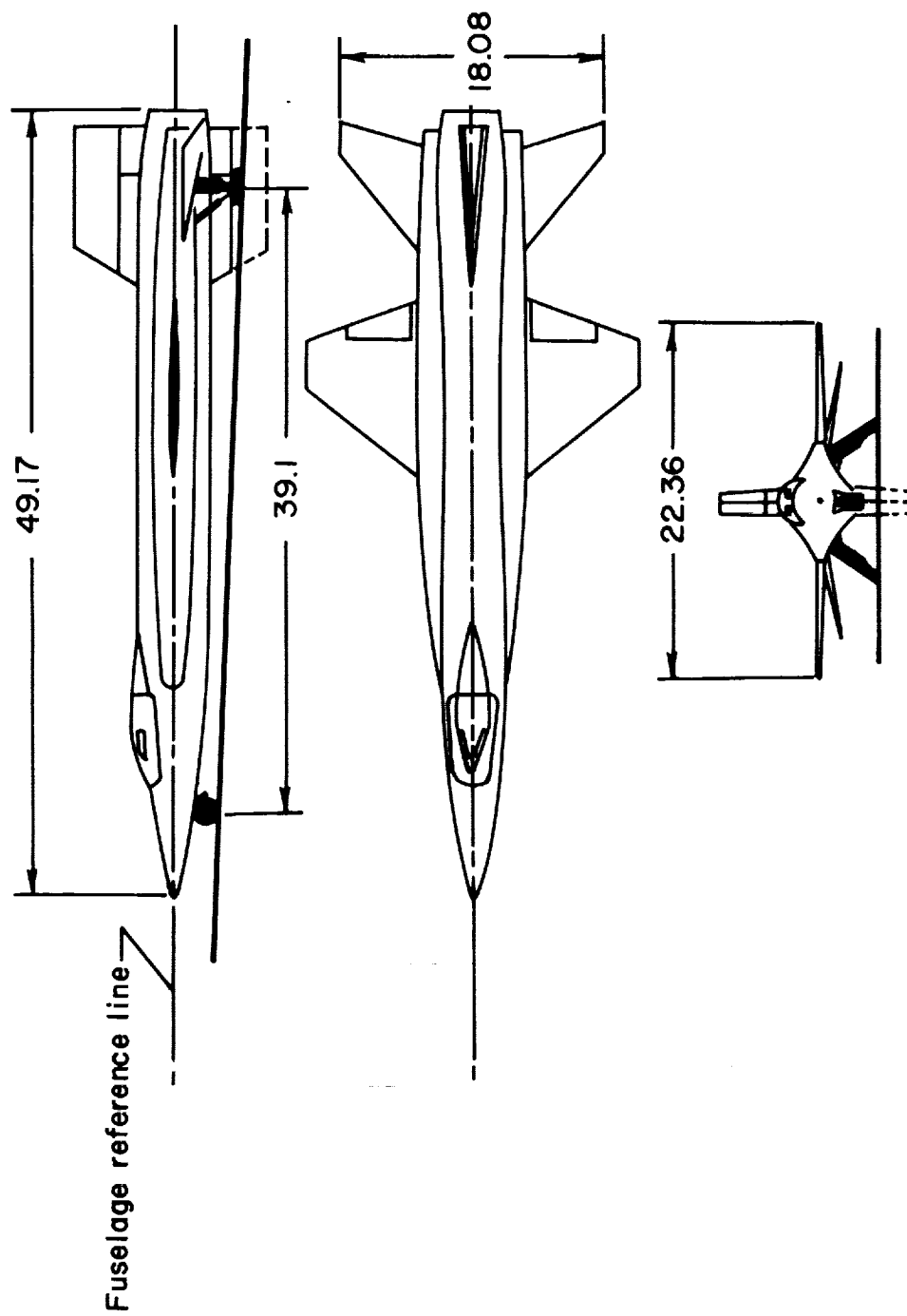
Figure 1.- Three-view drawing of the X-15 airplane. All dimensions in feet.

23

Figure 2.- Photograph of the X-15 airplane.
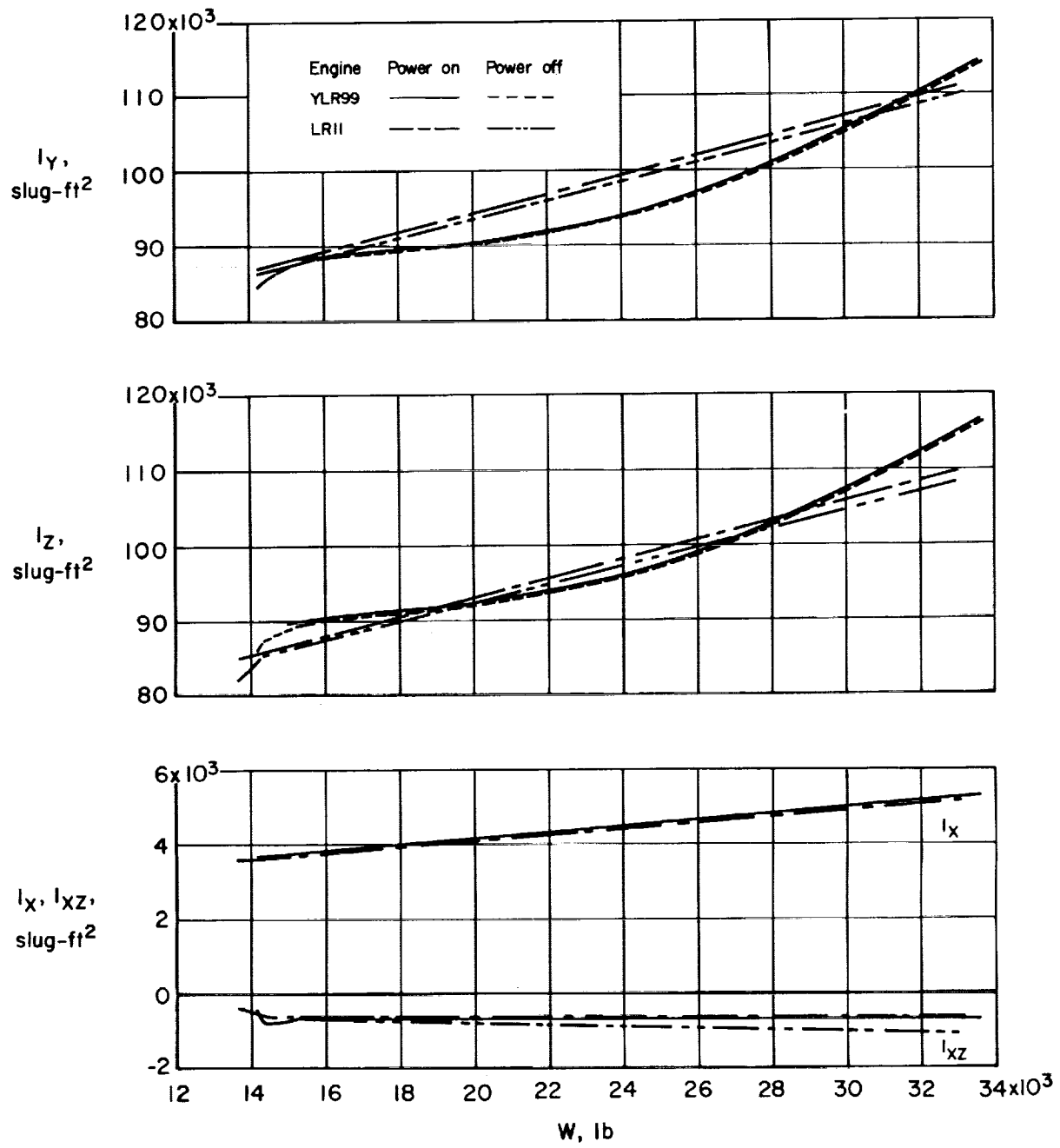
Figure 3.- Variation of inertia characteristics of the X-15 airplane with airplane weight (data supplied by manufacturer).

Figure 4.- The high-temperature flow-direction sensor installed on the nose of the X-15.
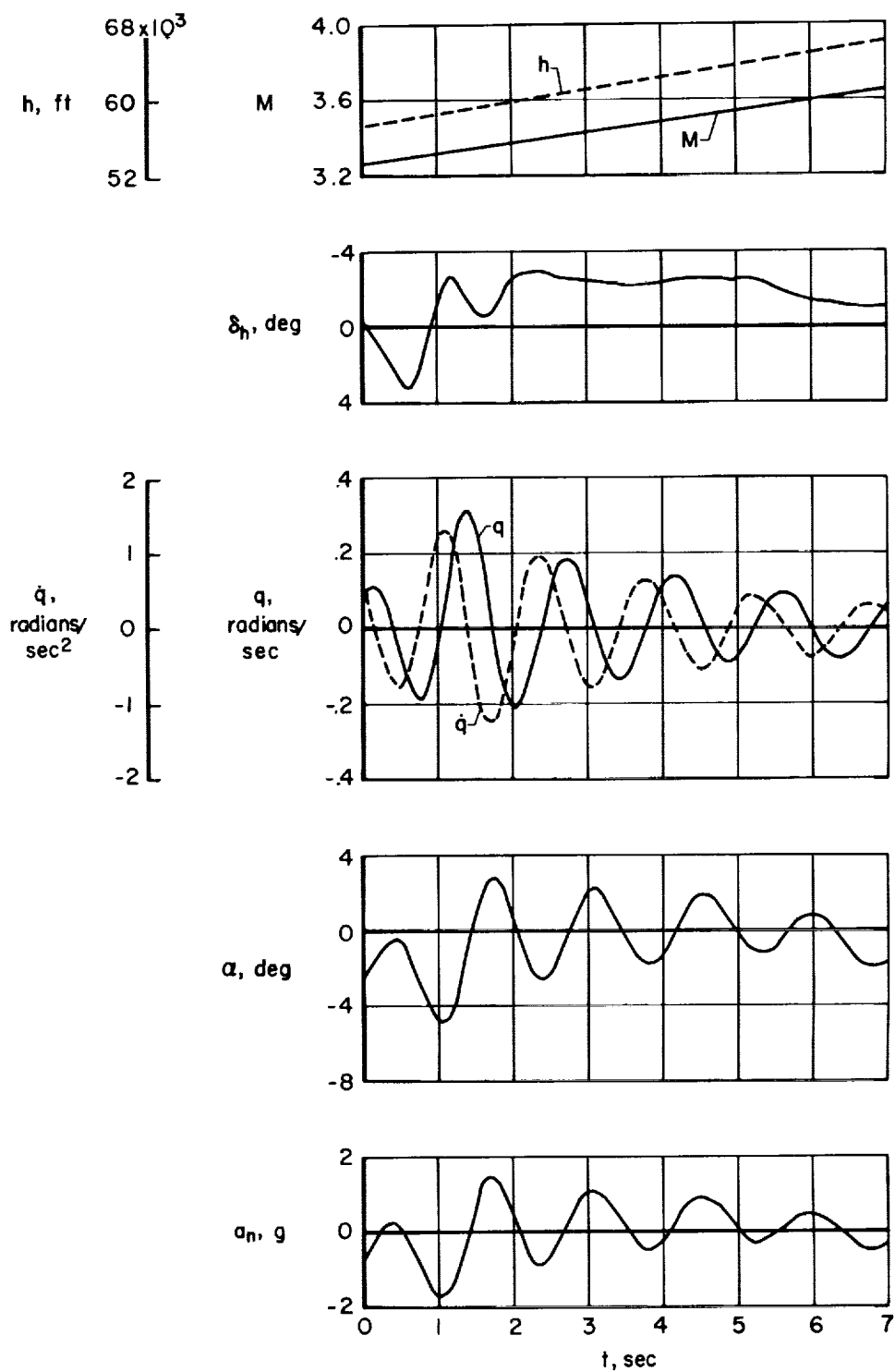
Figure 5.- Time history of longitudinal oscillations resulting from a stabilizer pulse. Power on; SAS gain settings of 0, 7, 8 for pitch, roll, and yaw, respectively.
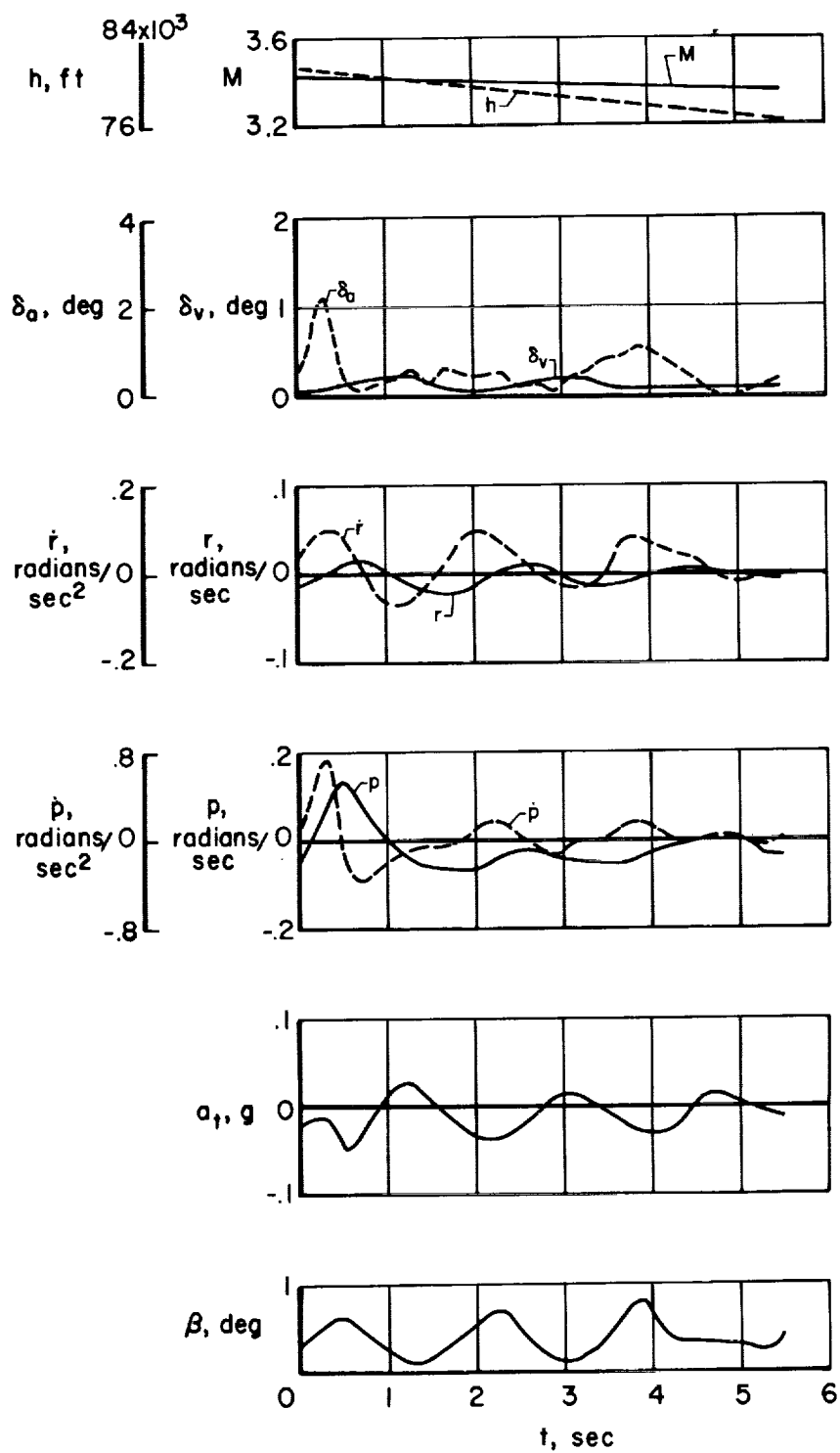
Figure 6.- Time history of lateral-directional response characteristics induced by an aileron input. Power off; SAS gain settings of 8, 6, 8 for pitch, roll, and yaw, respectively.

28
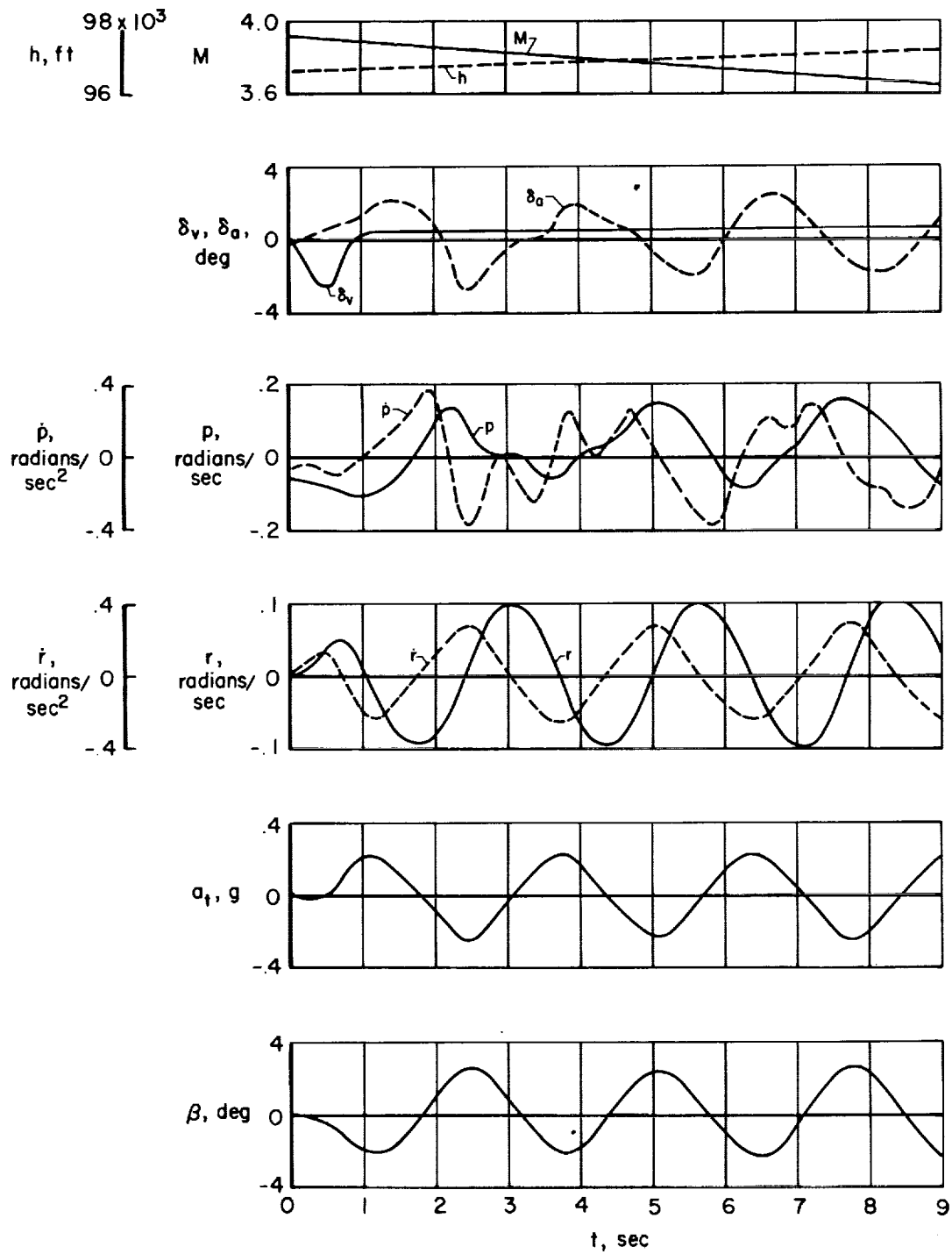
Figure 7.- Time history of lateral-directional response characteristics
resulting from a vertical-tail deflection. Power off; SAS gain
settings of 6, 6, 0 for pitch, roll, and yaw, respectively.
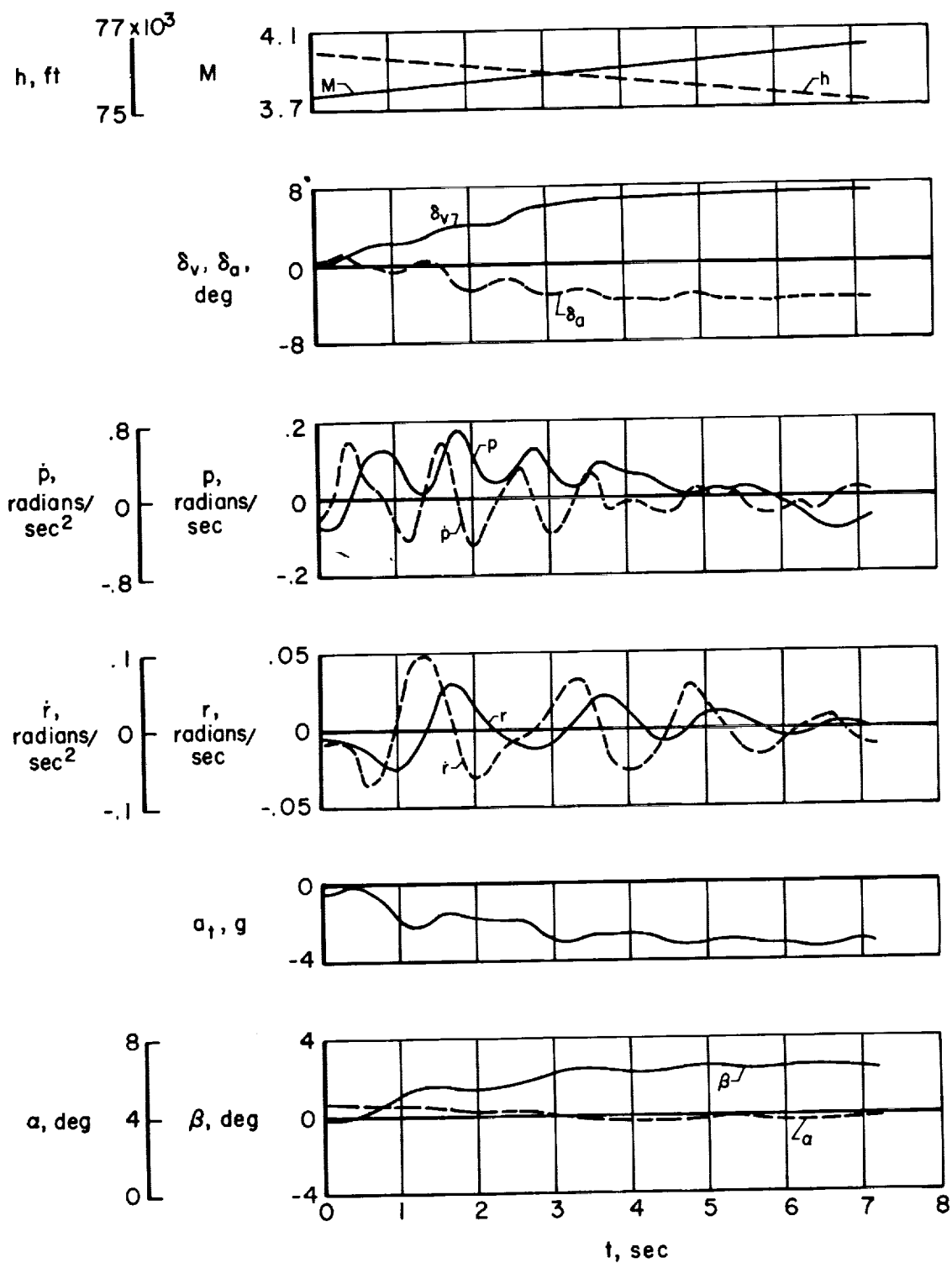
Figure 8.- Time history of a sideslip maneuver. Power on; SAS gain settings of 0, 4, 8 for pitch, roll, and yaw, respectively.
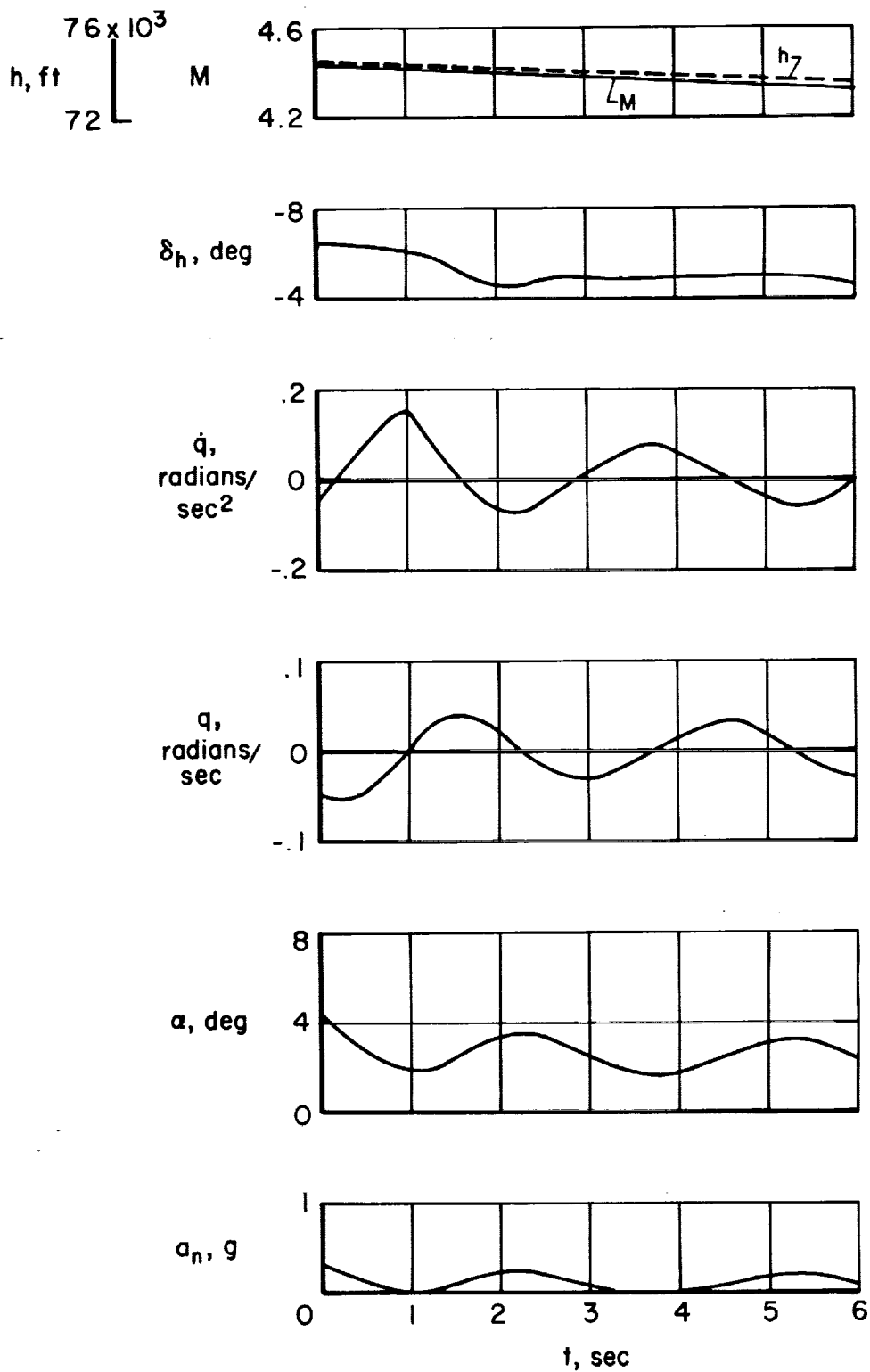
Figure 9.- Time history of random longitudinal oscillations. Power off; SAS
gain settings of 0, 4, 8 for pitch, roll, and yaw, respectively.
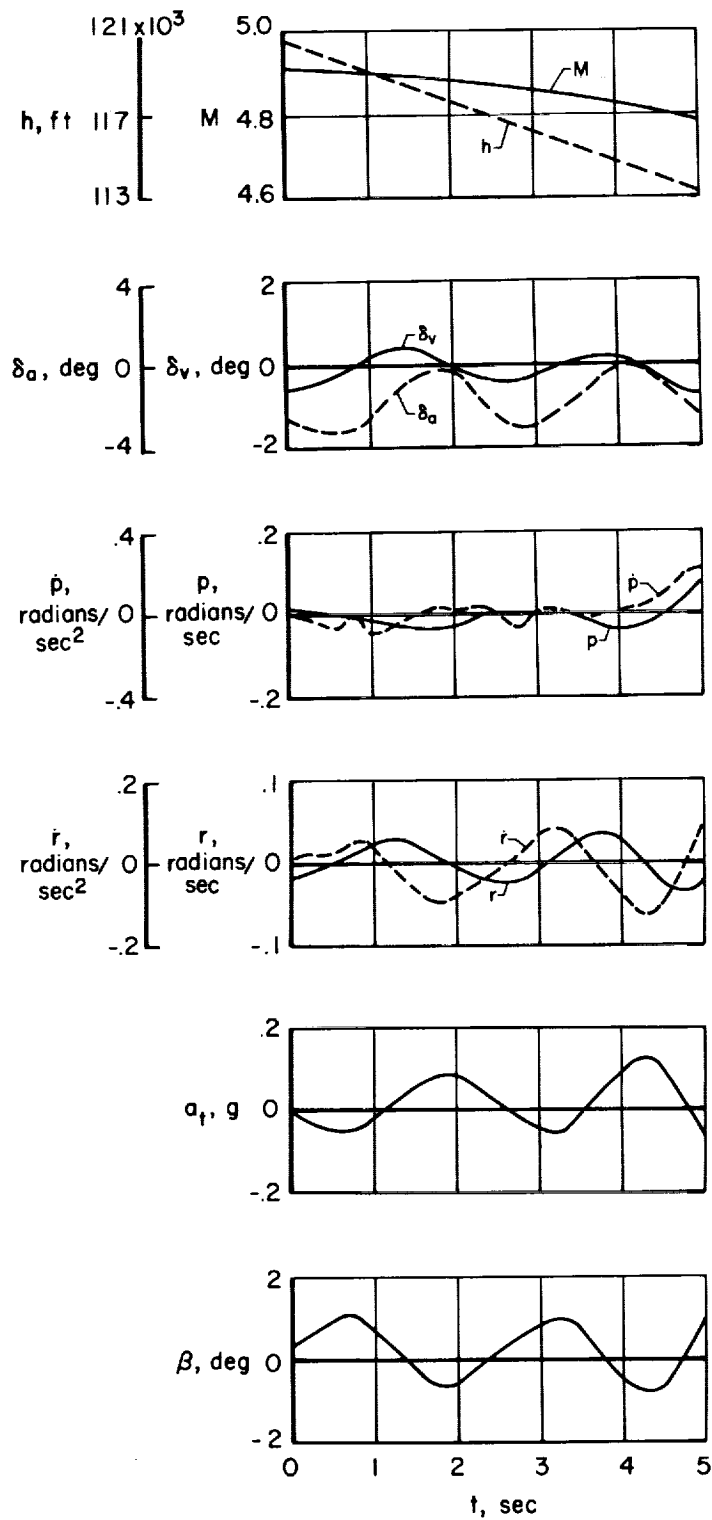
Figure 10.- Time history of random lateral-directional oscillations.
Power off; adaptive gain in pitch and roll, and fixed gain in yaw.
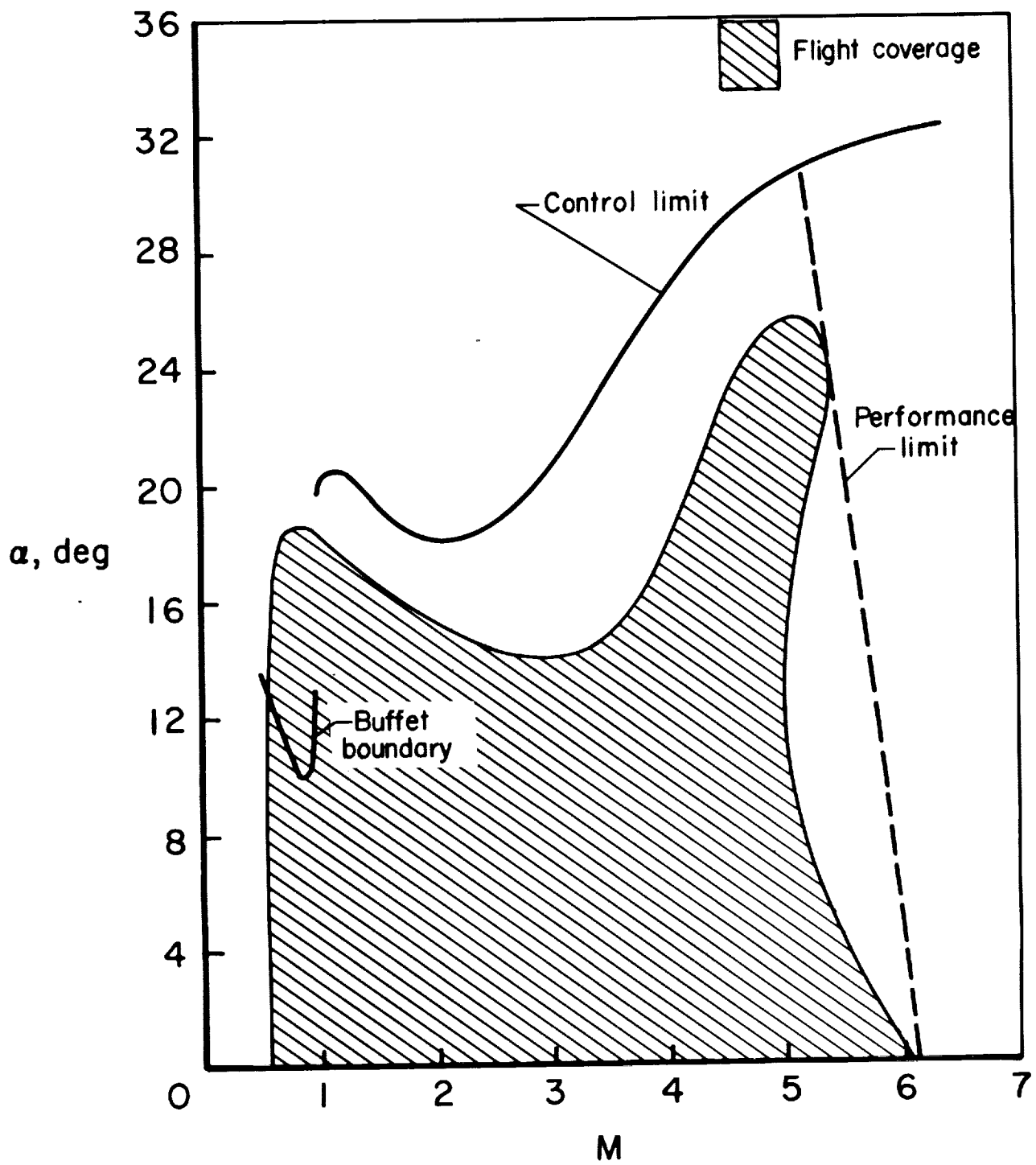
Figure 11.- Flight coverage of X-15 stability and control derivatives.
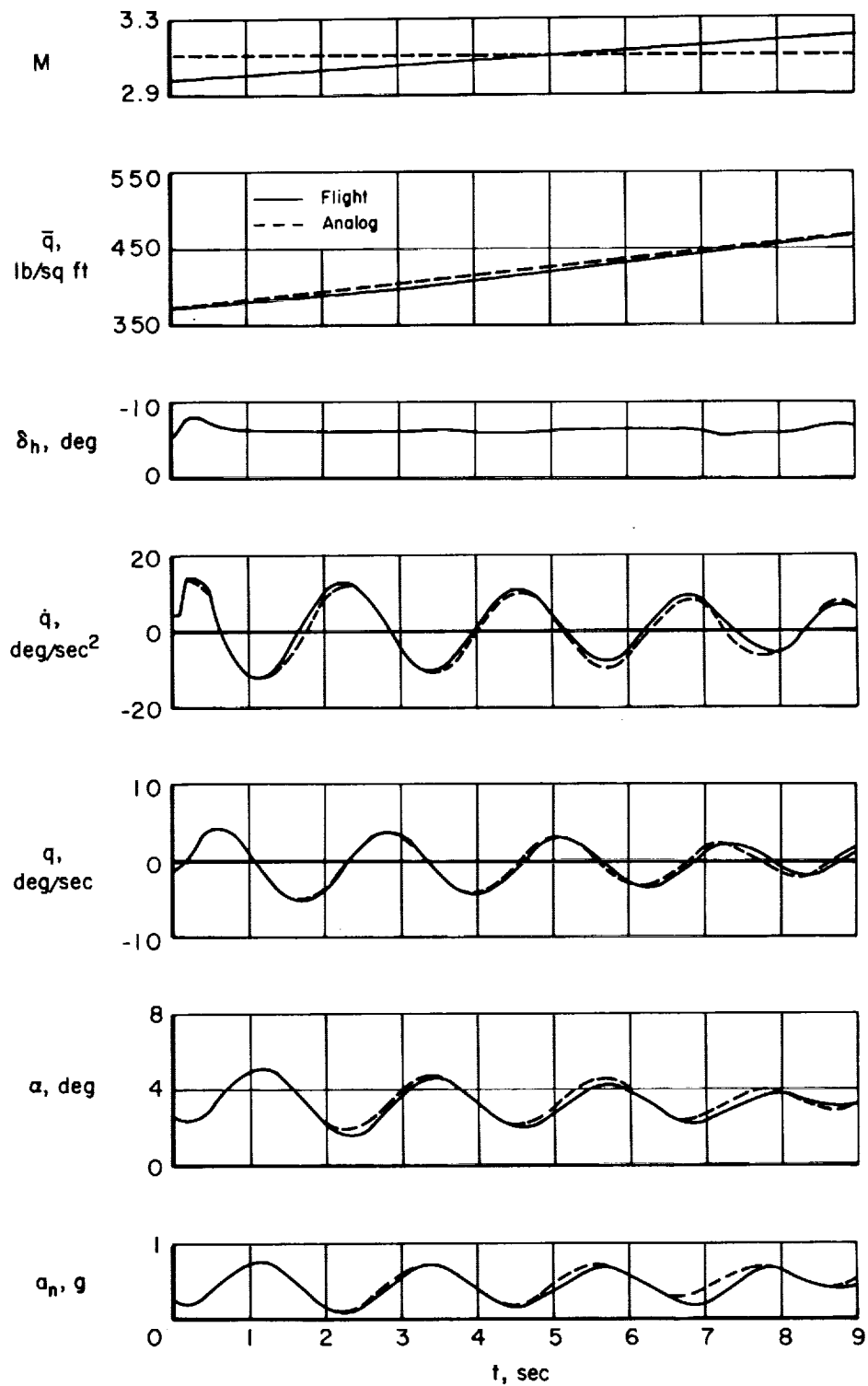
Figure 12.- Analog match of a pitch pulse. Power on; SAS gain settings of 0, 4, 8 for pitch, roll, and yaw, respectively.
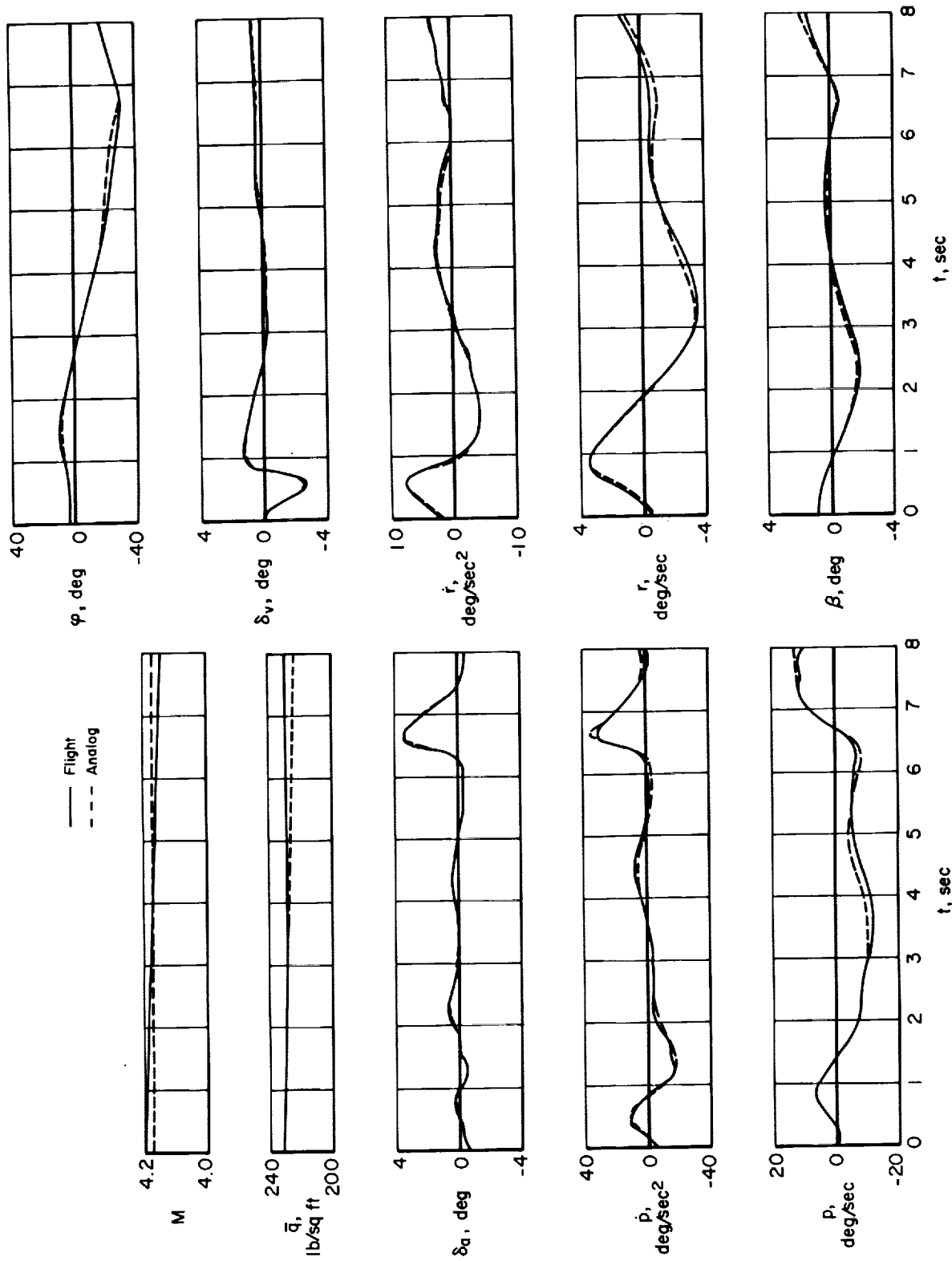
Figure 13.- Analog match of a yaw pulse. Power off; SAS gain settings of 8, 6, 8 for pitch, roll, and yaw, respectively.

35
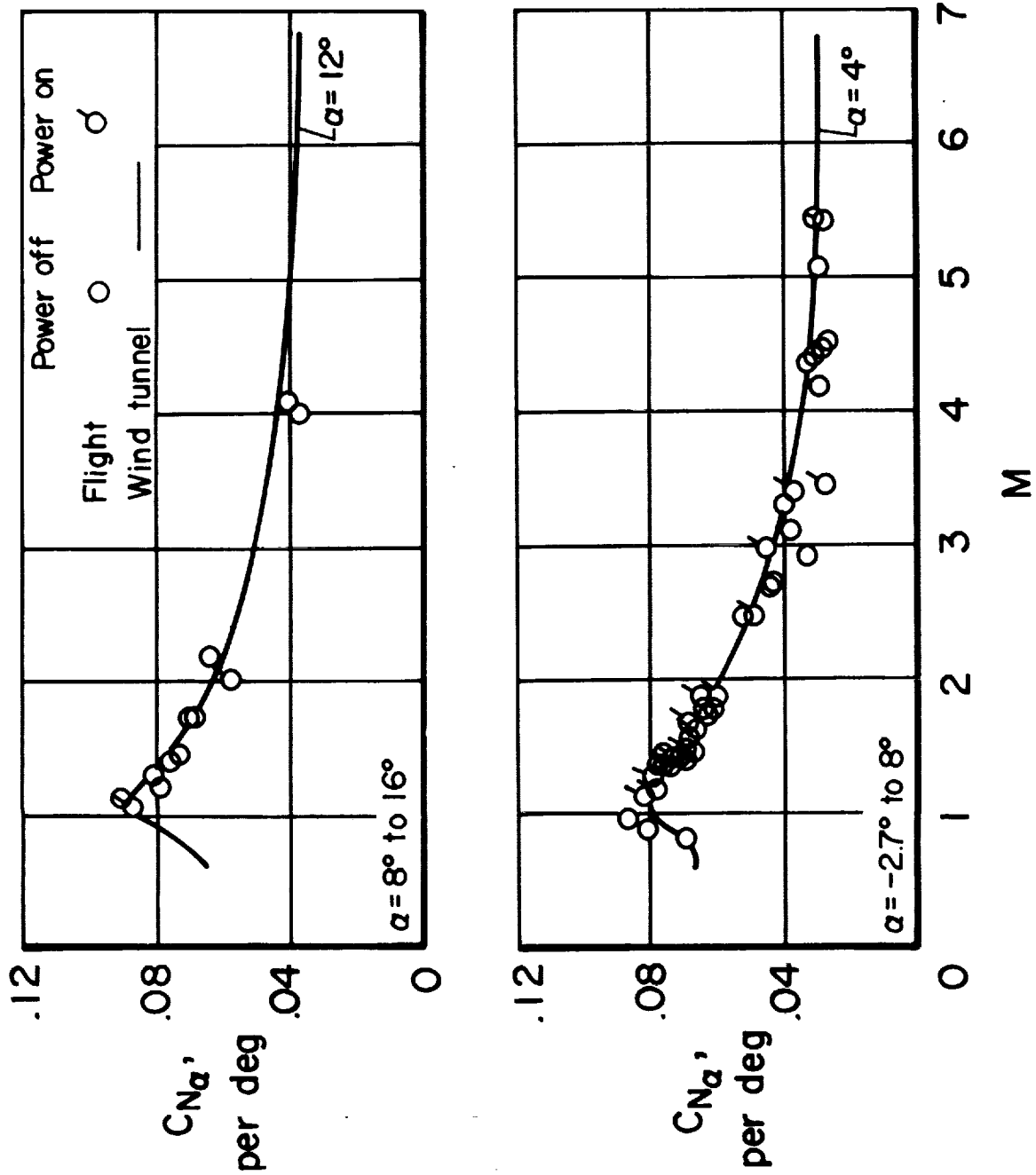
Figure 14.- Variation of normal-force-curve slope with Mach number.
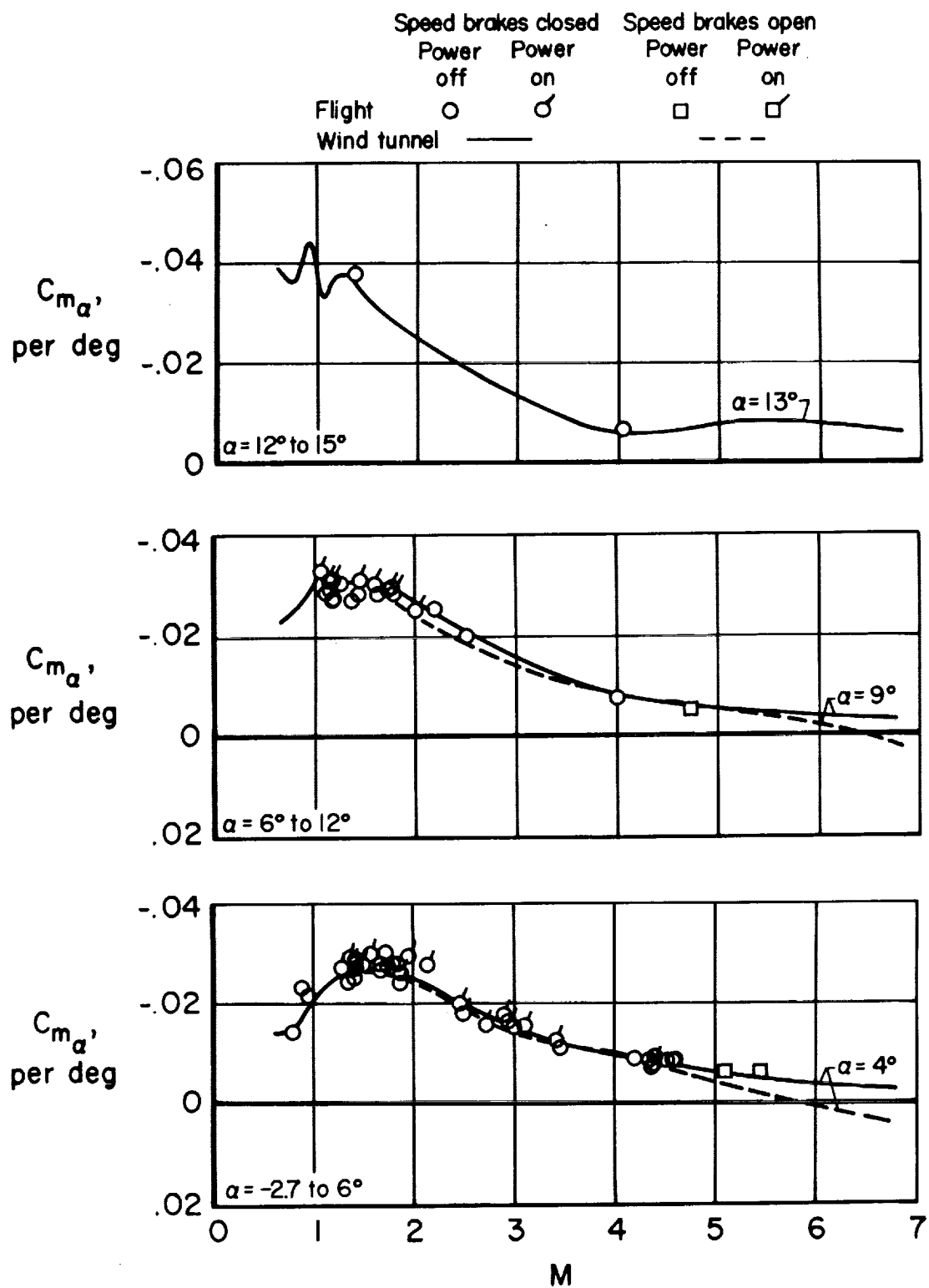
Figure 15.- Variation of longitudinal-stability derivative with Mach number.
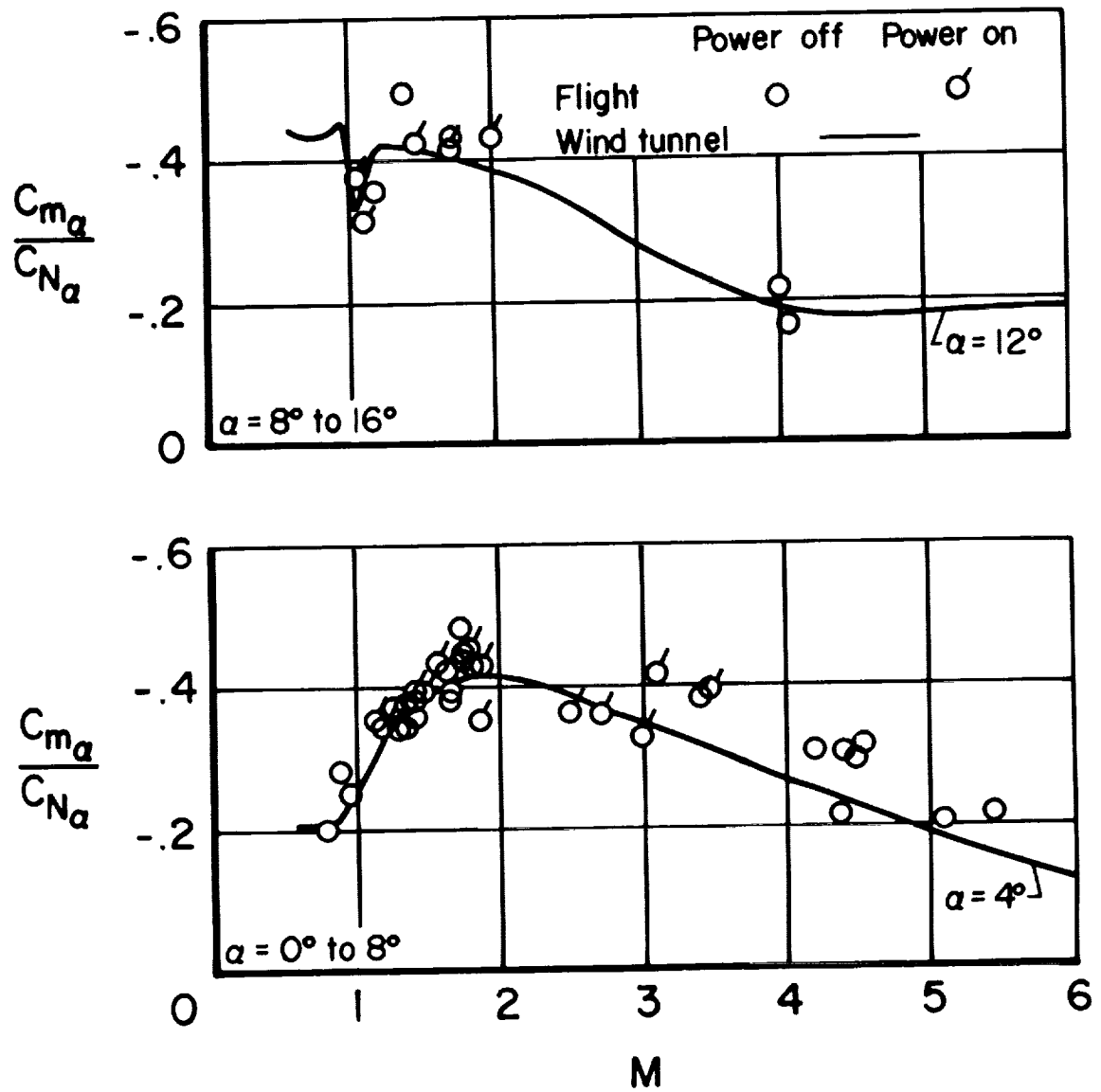
Figure 16.- Variation of static-margin parameter with Mach number.

38
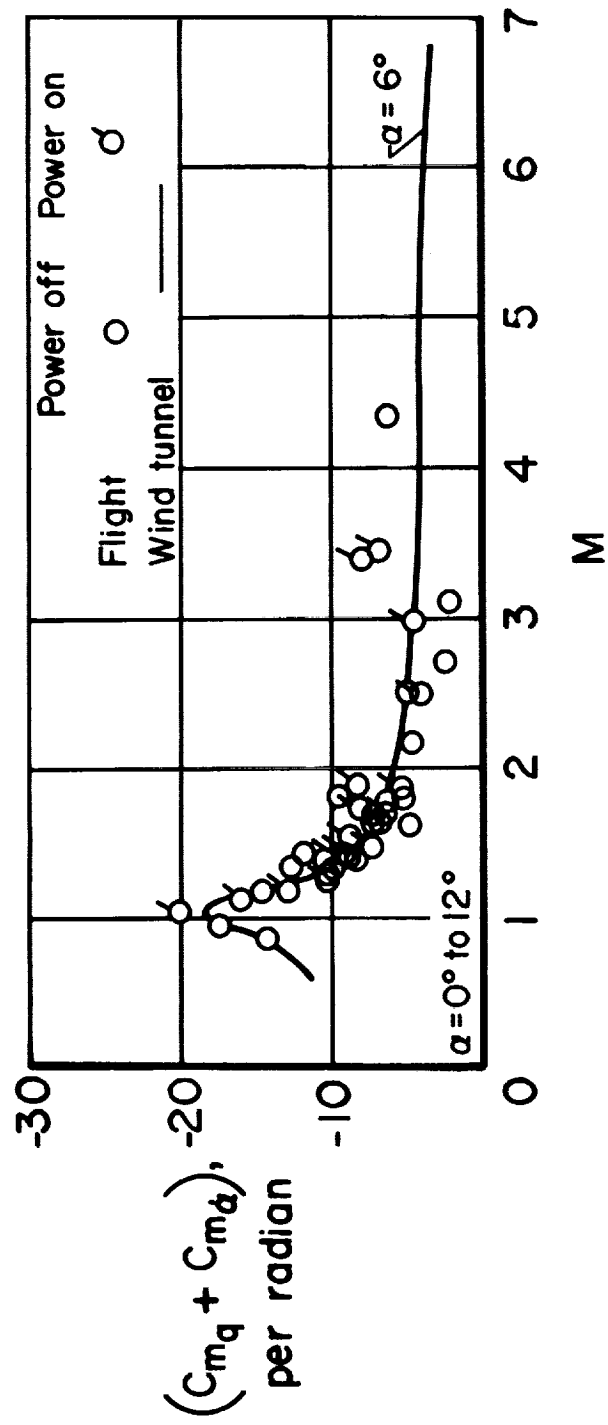
Figure 17.- Variation of pitch-damping derivative with Mach number.
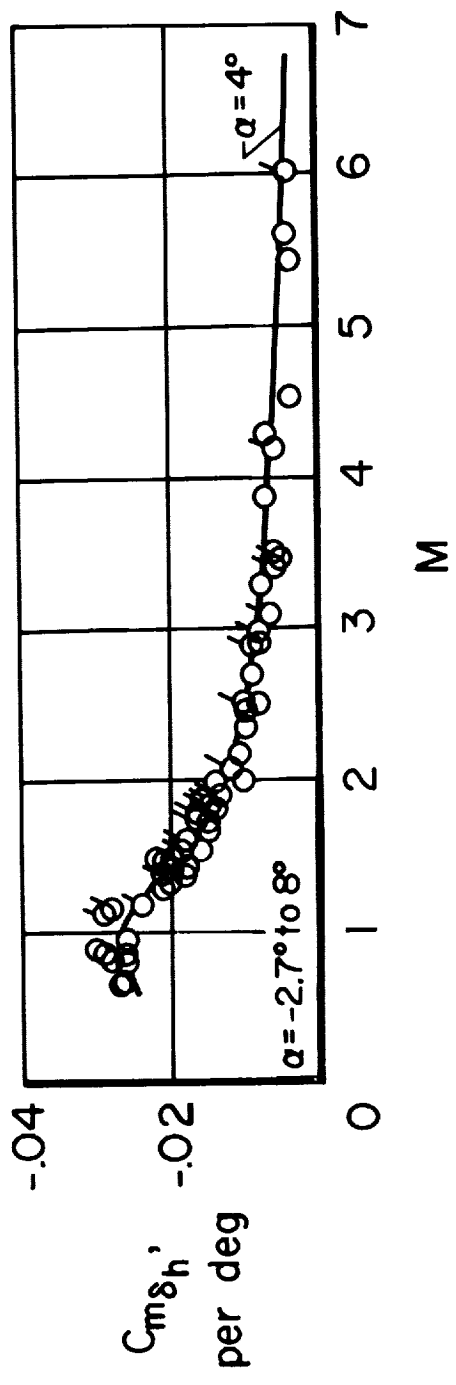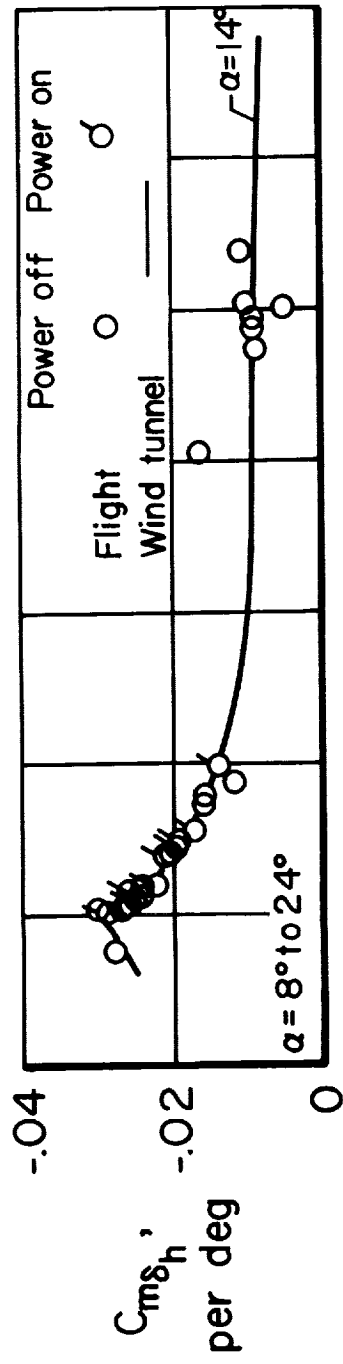
Figure 18.- Variation of longitudinal-control derivative with Mach number. $\delta_h = 0°$ to $-20°$.
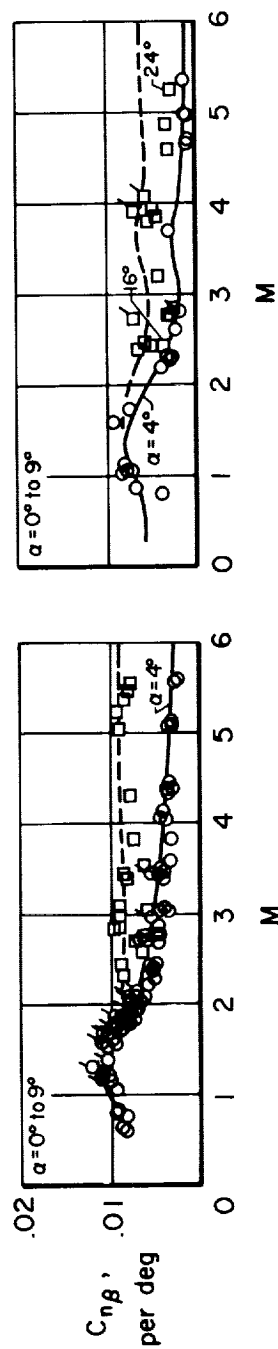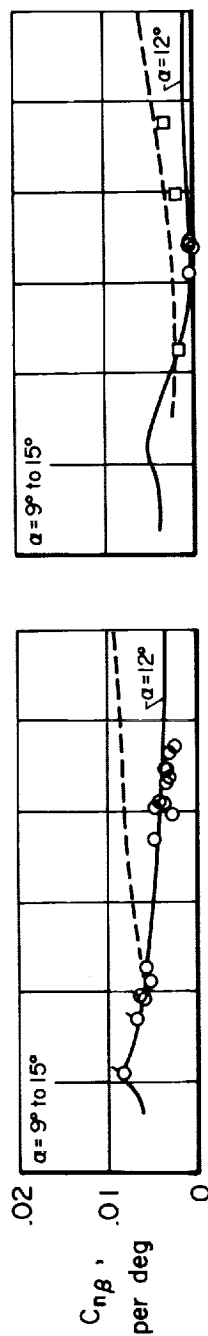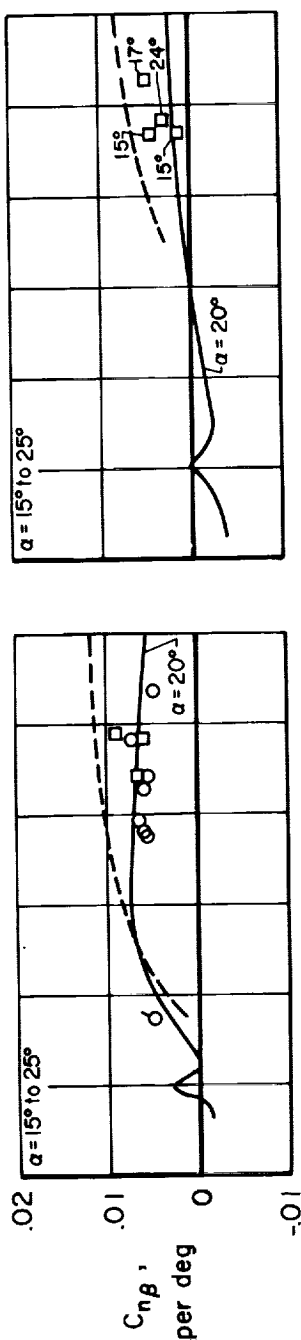
(a) Lower rudder on.

(b) Lower rudder off.

Figure 19.- Variation of directional-stability derivative with Mach number.

41

(a) Lower rudder on.
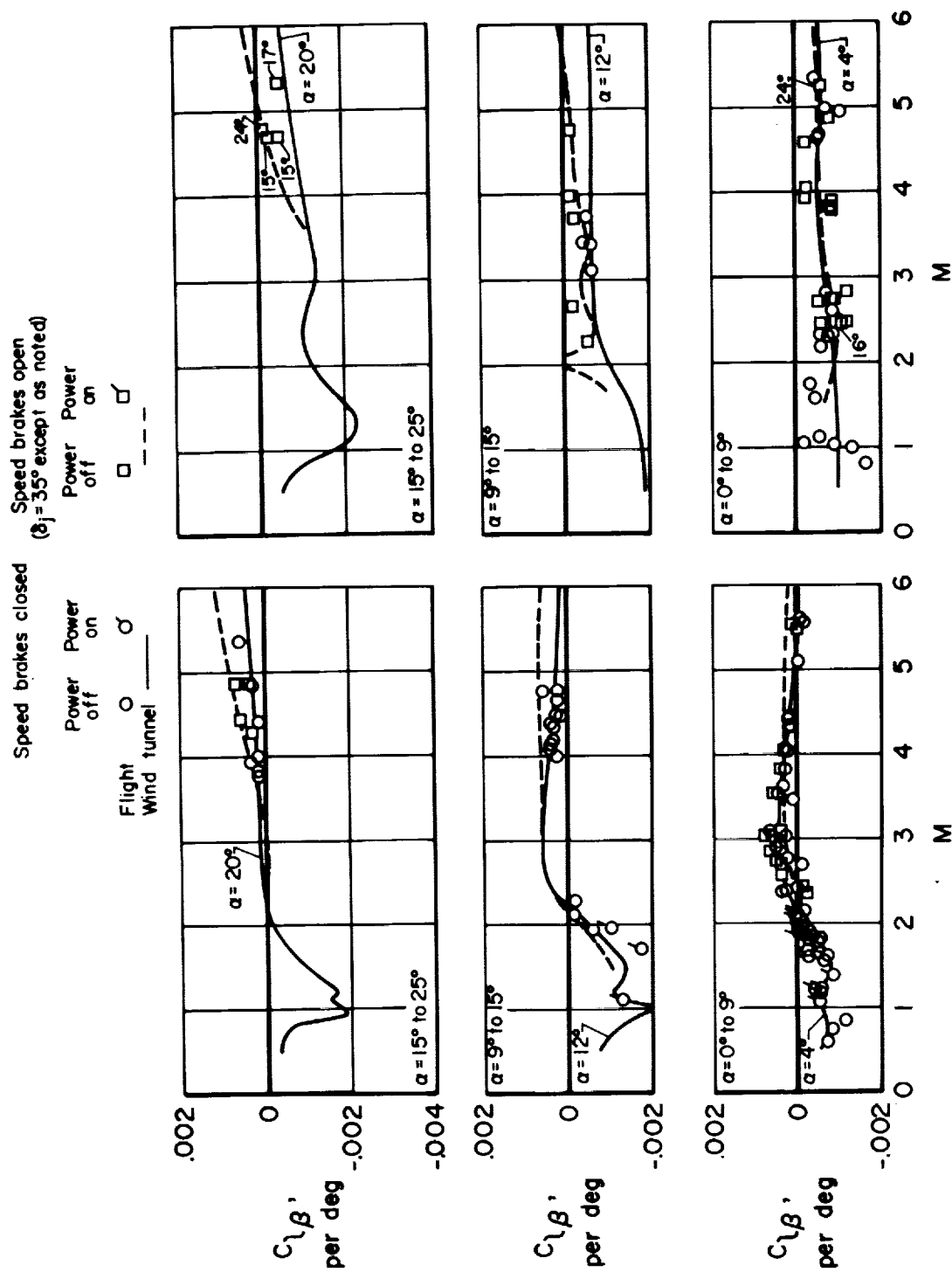
(b) Lower rudder off.

Figure 20.- Variation of effective-dihedral derivative with Mach number.
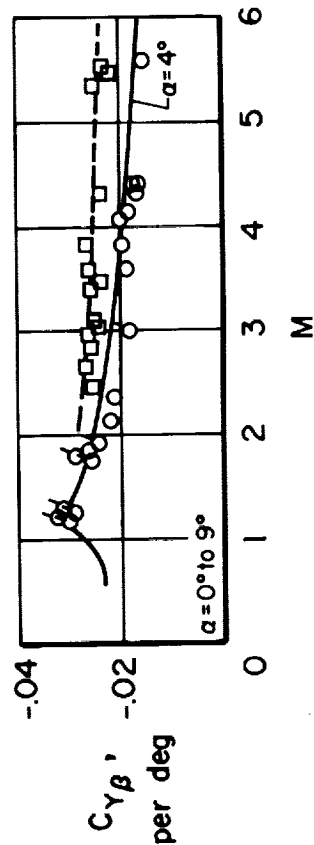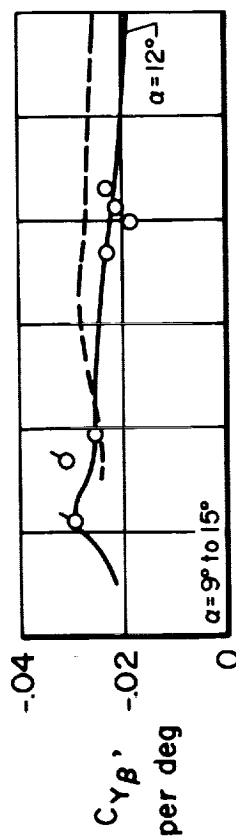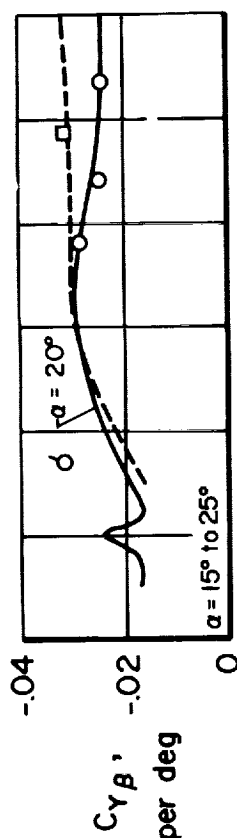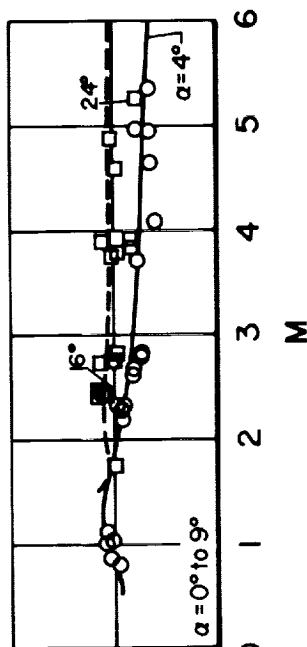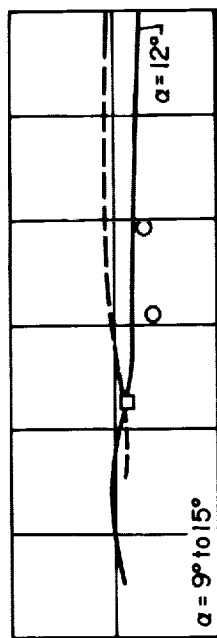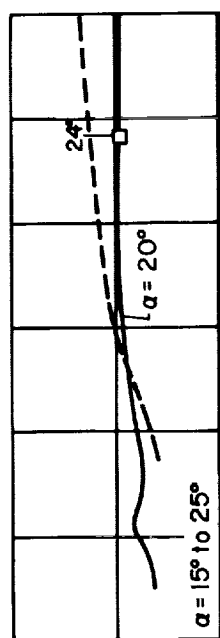
Figure 21.- Variation of side-force derivative with Mach number.

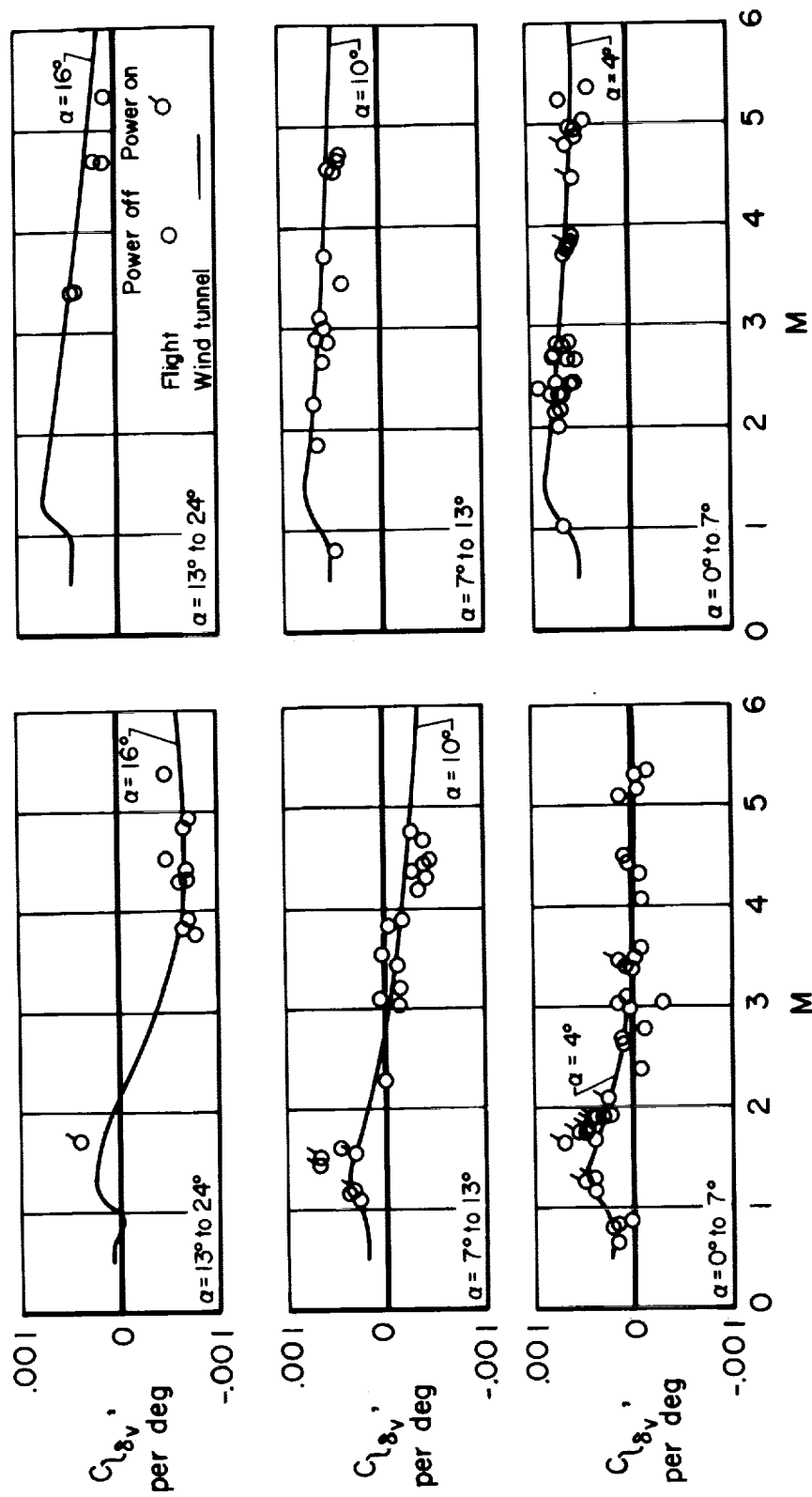(a) Lower rudder on.
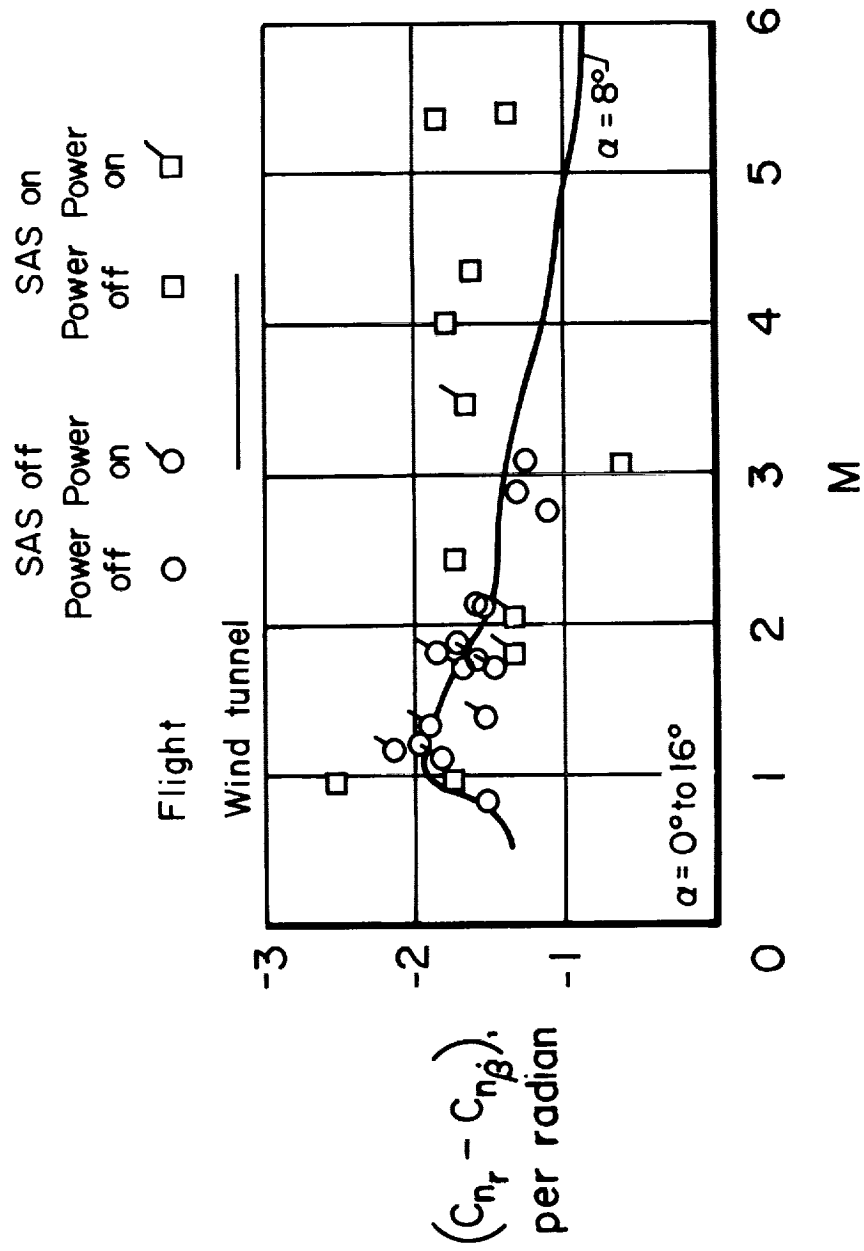
(b) Lower rudder off.

Figure 22.- Variation of damping-in-yaw derivative with Mach number; lower rudder on.
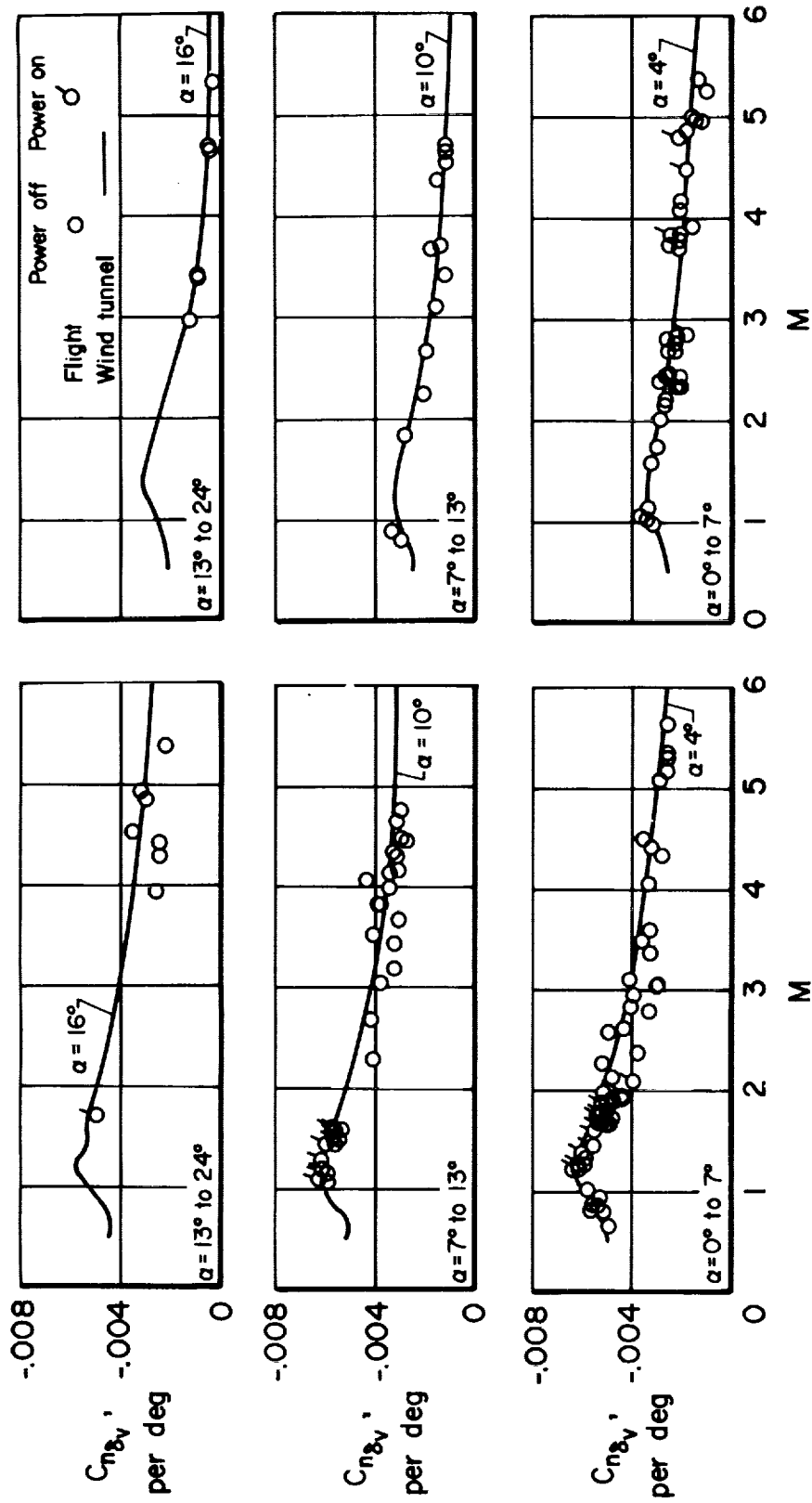
(a) Lower rudder on.

(b) Lower rudder off.

Figure 23.- Variation of directional-control derivative with Mach number.

(a) Lower rudder on.

(b) Lower rudder off.

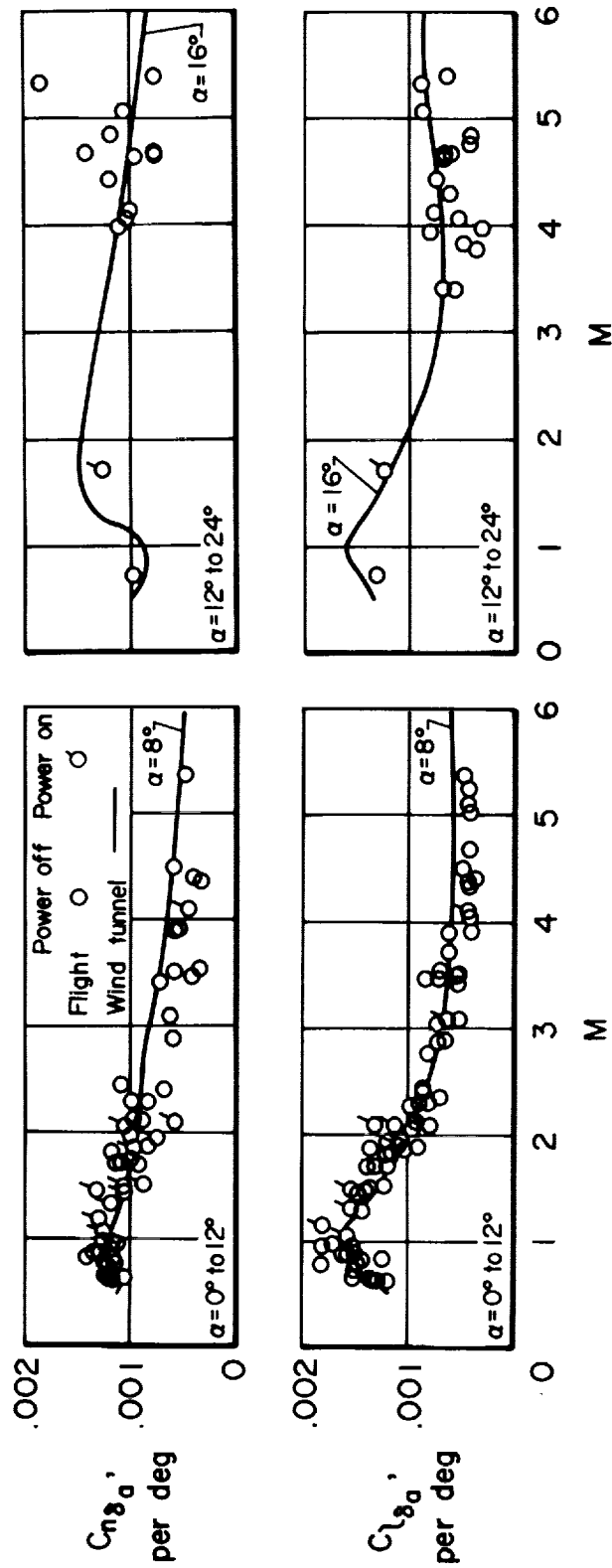Figure 24.- Variation of directional cross-control derivative with Mach number.

Figure 25.- Variation of roll-control derivatives with Mach number.